1971

Study of the mass and charge transport in thoria

Nabendu Sekhar Choudhury
Iowa State University

Study of the mass and charge transport in thoria

by

Nabendu Sekhar Choudhury

A Dissertation Submitted to the

Graduate Faculty in Partial Fulfillment of

The Requirements for the Degree of

DOCTOR OF PHILOSOPHY

Major Subject: Metallurgy

Approved:

Signature was redacted for privacy.

In Charge of Major Work

Signature was redacted for privacy.

Head of Major Department

Signature was redacted for privacy.

Dean of Graduate College

Iowa State University
Of Science and Technology
Ames, Iowa

1971

TABLE OF CONTENTS

INTRODUCTION

General Remarks

The phenomenon of charge conduction by mass transport in a solid medium was, perhaps, first observed by Sir Humphrey Davy (1), who in 1807 electrolyzed solid potassium hydroxide to isolate potassium metal. As early as 1899 W. Nernst (2) demonstrated that the electrical conduction in a zirconia-yttria solid solution is primarily due to mobile oxygen ions.

The ideas concerning various kinds of defects in thermal and chemical equilibrium in an ionic crystal were developed by Frenkel (3) and Wagner and Schottky (4). It was Wagner's classical paper (5) in 1933 concerned with the theory of oxidation of metals, which elucidated that these defects are responsible for the transport of charge and mass through an ionic compound. In that paper (5) Wagner formulated the generalized transport equations for charged species and laid the foundation for the study of the defect chemistry of ionic compounds by electrochemical techniques. The direct implications of Wagner's classical work were the following:

(1) The experimentally observed high temperature parabolic scaling (oxidation) rate constant may be quantitatively correlated with the mixed conduction (i.e. charge conduction by ions, electrons in the conduction band which will be referred to as excess electrons, and holes in the valence band) properties of the scaling layer, and

(2) Quantitative expression of the open circuit emf, generated across a mixed conductor, may be written explicitly in terms of its ionic

transference number* and the metal and/or non-metal component chemical potentials established at the electrodes.

These important derivations are worked out in Appendix A-1.

Solid Electrolytes and Their Applications

Applications of Wagner's theory were largely limited to oxidation studies until 1957, when Kiukkola and Wagner (6,7) revived interest on the class of mixed conductors known as solid electrolytes (i.e. those having ionic transference number very close to unity). In their work they determined the free energy of formation of several binary oxides using a solid electrolyte (calcia stabilized zirconia) galvanic cell technique.

Following Kiukkola and Wagner's work solid electrolytes drew the attention of many investigators and were used in various applications. Extensive reviews involving solid electrolytes and their applications have been published by Alcock (8), Raleigh (9) and Rapp and Shores (10). The reader is also referred to an excellent discussion of the applications of solid electrolytes by Schieltz (11).

Research applications of solid electrolytes are extensive and include

---

*The transference number of jth charge carrier is defined as the ratio of partial jth carrier conductivity to the total conductivity i.e.

$$t_j = \frac{\sigma_j}{\sum_{\text{all carriers}} \sigma_i}$$

where t_j = transference number of jth carrier

σ_i = partial conductivity of the ith carrier.

a variety of thermodynamic and kinetic studies. Practical applications, involving solid electrolytes, are natural extensions of these thermodynamic and kinetic studies. The essential requirement, for all such applications, is that the ionic transference number of the solid electrolyte must be very close to unity, in which case, Equation [A-1.28] in Appendix A-1 reduces to

$$-\frac{(\mu_{X_2}'' - \mu_{X_2}')}{2 Z_2 F} = -\frac{(\mu_M'' - \mu_M')}{Z_1 F} = (\Phi'' - \Phi') \qquad [1]$$

It is apparent from Equation [1] that, if the metal or the non-metal chemical potential at one end of the electrolyte is known, the chemical potential at the other end may be determined from the observed emf. This is the basic principle involved in all thermodynamic (galvanic cell) measurements involving solid electrolytes. Solid electrolyte galvanic cells have been used in a wide variety of research applications. The following partial listing gives typical examples:

(a) Determination of the free energies of formation of various oxides, halides and spinels (6,7,12-18)

(b) Studies involving phase relationships (19)

(c) Determination of the thermodynamic activity of a metal in an alloy (20,21)

(d) To monitor the oxygen content in molten metal and solid metallic solutions (22-24).

The idea of monitoring oxygen content in molten steel by solid electrolyte galvanic cell technique has prompted considerable research

sponsored by the steel industry. Varying degrees of success have been achieved in this connection (22,24). The ability of an oxygen conducting solid electrolyte to monitor oxygen partial pressure in vacuum or gaseous atmosphere has led to the development of various commercially available oxygen pressure gages (25).

The major attention on solid electrolytes by the commercial and military interests was focussed during the past decade with a view to develop solid electrolyte fuel cells or batteries for the direct conversion of chemical energy to electrical energy (26,27). Various experimental fuel cells with solid electrolytes have been constructed (28,29). However, commercial solid electrolyte fuel cells and batteries are still in the process of development.

The kinetic studies involving solid electrolytes are based on the following two principles:

(1) an emf-applied to a solid electrolyte by means of a reversible electrode (i.e. the electrode which maintains a fixed chemical potential) on one side and a non-reversible electrode on the other side controls the chemical potential at the non-reversible electrode; and

(2) the measured current flowing through the electrolyte is equivalent to the flux of mobile ions passing to or from the non-reversible electrode; i.e. neglecting electronic currents the measured current gives the reaction rate at the non-reversible electrode.

The diffusion coefficients of oxygen in solid copper (30) and solid silver (30-33) have been determined in this way. Similarly Raleigh (34-36) determined the diffusion coefficient of Ag in solid Ag-Au alloys

using solid AgBr electrolyte. Rickert (37) has reviewed several other important kinetic studies involving solid electrolytes. Tare and Schmalzried (38) determined the phase-boundary reaction rates for the oxidation of a thin iron foil in various CO/CO_2 atmospheres and also were able to determine the supersaturation necessary to nucleate wüstite in the iron foil.

A direct practical application suggested by such kinetic studies is that of a solid electrolyte ion pump i.e. the possibility of pumping a given species into or out of a chamber enclosed by the solid electrolyte. Although practical solid electrolyte ion pumps are yet to be perfected, it should, in principle, be possible to utilize this ion pump concept in such applications as purification of metals or in the construction of controlled atmosphere furnace tubes. Yuan and Kröger (39) have used a calcia-stabilized zirconia electrolyte as an ion pump to coulometrically titrate oxygen from stationery and flowing gases. Tretyakov and Muan (40) utilized the principle of coulometric titration of oxygen for electrochemical investigation of yttria doped thoria.

Properties of Solid Electrolytes

The uses of ionic conductors in various solid-electrolyte applications are largely limited by:

(1) The rather high resistance of solid electrolytes, and

(2) The onset of hole (p-type) and excess electronic (n-type) conduction at high and low non-metal chemical potentials respectively.

It should be noted that most ionic solids (especially most of the

oxides e.g. Cu_2O, NiO, FeO, CoO etc.) are predominantly electronic conductors (either p-type or n-type). Thus there are only limited numbers of predominantly ionic conductors and the onset of p-type or n-type conduction further limits the application of such a material as solid electrolyte. Thus the useful range of non-metal chemical potential of a solid electrolyte is the range where the ionic conductivity is much larger than the p-type or the n-type conductivity so that the ionic transference number is essentially unity within that range.

In all known solid electrolytes the ionic conductivities are found to be independent of P_{X_2}, the non-metal gaseous dimer (X_2 gas) partial pressure. In contrast, however, the p-type and the n-type electronic conductivities are proportional to $P_{X_2}^{+1/n}$ and $P_{X_2}^{-1/n}$ respectively, where the quantity n empirically characterizes the observed P_{X_2} dependences. Alternatively the value of n may be theoretically evaluated by assuming that the conductivities are proportional to the carrier concentrations. The concentrations and hence the partial conductivities are then related to P_{X_2}, first hypothesizing various defect equilibria and then combining the corresponding mass action equations with the condition of charge neutrality and the assumption of ideal solution behavior. For solid electrolytes this approach almost always leads to the prediction that $n = 2|Z_2|$ where Z_2 is the valence of the anions in the electrolyte. However other values for n have also been deduced (41). Kröger and Vink (42) have given the general description of the concentration variations of different charge carriers as functions of P_{X_2} and have summarized them in the form of "Kröger and Vink" diagrams. The region of "Kröger

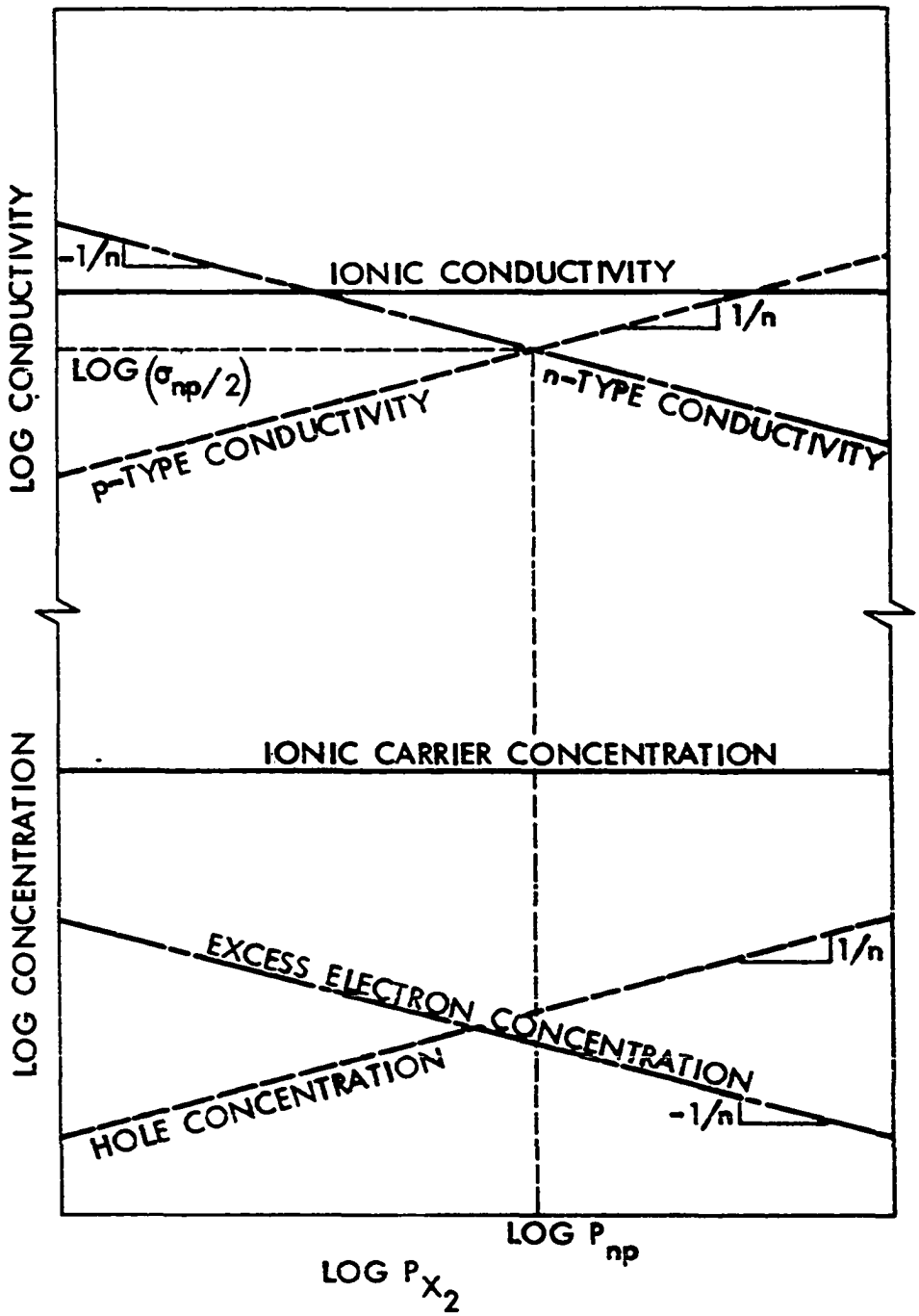

Figure 1. "Kröger and Vink" diagram for a predominantly ionic conductor

and Vink' diagram, for an ionic crystal where the concentration of ionic charge carriers are predominant, is given in Figure 1. In this region, the ionic charge carrier concentration is P_{X_2} independent; however, this is not true at extremely high or low P_{X_2} where the hole or the excess electronic carrier concentration predominates. In those regions the mass action analysis (43) predicts the ionic carrier concentration to be P_{X_2} dependent.

The mobilities of ionic carriers are generally three orders of magnitude lower than that of the excess electrons and holes. Therefore, the magnitude of the electronic or the hole conductivity becomes comparable with the ionic conductivity even when the ionic carrier concentration is much larger than the electron or hole concentration. The partial ionic, electronic and hole conductivities are also schematically illustrated in Figure 1.

Following Schmalzried's terminology (44,45) $P_{\oplus}$ and $P_{\ominus}$ are the P_{X_2} values at which the hole and the electronic conductivities are respectively equal to the ionic conductivity. Within the range of P_{X_2}, where the concentrations of ionic charge carriers are constant (i.e. independent of P_{X_2}), $\sigma_{\oplus}$ the p-type conductivity and $\sigma_{\ominus}$ the n-type conductivity may be expressed in terms of P_{X_2}, $P_{\oplus}$, $P_{\ominus}$ and the ionic conductivity σ_{ion} as follows

$$\sigma_{\oplus} = \sigma_{ion} P_{\oplus}^{-1/n} P_{X_2}^{1/n} \qquad [2]$$

$$\sigma_{\ominus} = \sigma_{ion} P_{\ominus}^{1/n} P_{X_2}^{-1/n} \qquad [3]$$

The ionic transference number is then given by

$$t_{ion} = \frac{1}{1 + P_{\oplus}^{-1/n} P_{X_2}^{1/n} + P_{\ominus}^{1/n} P_{X_2}^{-1/n}} \qquad [4]$$

When $P_{\oplus} \gg P_{\ominus}$ and the ambient P_{X_2} is close to $P_{\oplus}$, t_{ion} may be approximated as

$$t_{ion} = \frac{1}{1 + P_{\oplus}^{-1/n} P_{X_2}^{1/n}} \qquad [5]$$

because $P_{\ominus}^{1/n} P_{X_2}^{-1/n}$ is negligible under these circumstances. Accordingly t_{ion} varies from essentially 0.5 at $P_{X_2} = P_{\oplus}$ to 0.99 at $P_{X_2} = (1/99)^n P_{\oplus}$, i.e. when P_{X_2} is 2n orders of magnitude lower than $P_{\oplus}$.

Similarly, when $P_{\ominus} \gg P_{\ominus}$ and the ambient P_{X_2} is close to $P_{\ominus}$, t_{ion} may be approximated by the relation

$$t_{ion} = \frac{1}{1 + P_{\ominus}^{1/n} P_{X_2}^{-1/n}} \qquad [6]$$

and the value of t_{ion} is essentially 0.5 when $P_{X_2} = P_{\ominus}$ and increases to 0.99 when the P_{X_2} is increased 2n orders of magnitude above $P_{\ominus}$.

By arbitrary convention the ionic transference number should be greater than or equal to 0.99 for most solid electrolyte applications (10). Therefore

$$\text{Log } P_{\oplus} - 2n \leq \text{Log } P_{X_2} \leq \text{Log } P_{\ominus} + 2n \qquad [7]$$

defines the useful P_{X_2} range for such applications. This range has been

labeled the electrolytic domain (46,47) for the mixed conductor in question.

In a solid electrolyte (at a constant ambient P_{X_2}) the ionic, the p-type and the n-type conductivities generally exhibit Arrhenius-type temperature dependence. Therefore, within the P_{X_2} range of constant ionic carrier concentration, the temperature and P_{X_2} dependences of these conductivities are given by

$$\sigma_{ion} = \sigma_{ion}^{o} \; e^{- Q_{ion}/RT} \qquad [8]$$

$$\sigma_{\oplus} = \sigma_{\oplus}^{o} \; P_{X_2}^{1/n_e} \; e^{- Q_{\oplus}/RT} \qquad [9]$$

$$\sigma_{\ominus} = \sigma_{\ominus}^{o} \; P_{X_2}^{-1/n_e} \; e^{- Q_{\ominus}/RT} \qquad [10]$$

where Q_{ion}, $Q_{\oplus}$ and $Q_{\ominus}$ characterize the activation energies for ionic, p-type and n-type conductions.

Equations [8], [9] and [10] may be combined to yield

$$P_{\oplus} = \left(\frac{\sigma_{ion}^{o}}{\sigma_{\oplus}^{o}} \right)^{n} e^{- n(Q_{ion} - Q_{\oplus}) \; / \; RT} \qquad [11]$$

$$P_{\ominus} = \left(\frac{\sigma_{ion}^{o}}{\sigma_{\ominus}^{o}} \right)^{-n} e^{-n \; (Q_{\ominus} - Q_{ion}) \; / \; RT} \qquad [12]$$

and

$$P_{np} = \left(\frac{\sigma_{\ominus}^{o}}{\sigma_{\oplus}^{o}} \right)^{n/2} e^{- n/2 \; (Q_{\ominus} - Q_{\oplus}) \; / \; RT} \qquad [13]$$

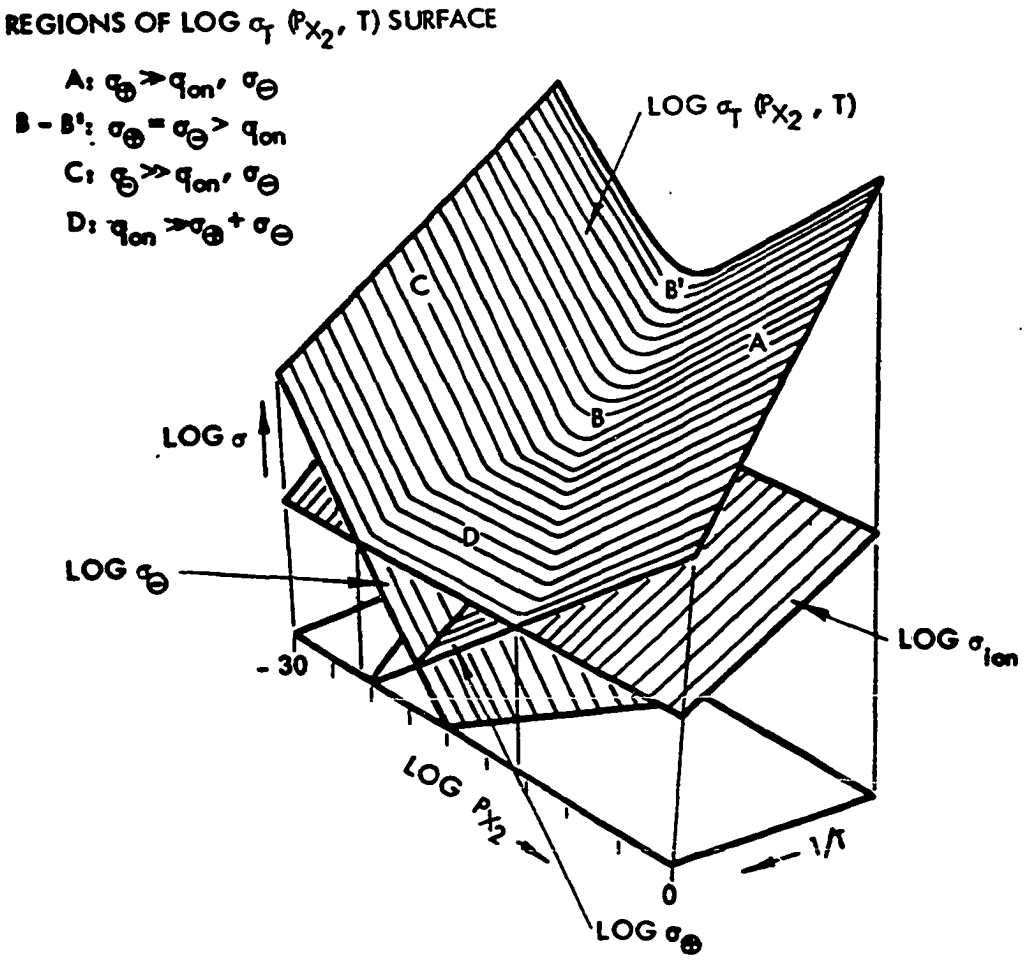

Figure 2. Schematic representation of Log σ surfaces over Log P_{X_2}, 1/T space for $\sigma = \sigma_{ion}, \sigma_\oplus, \sigma_\ominus$ and σ_{total}

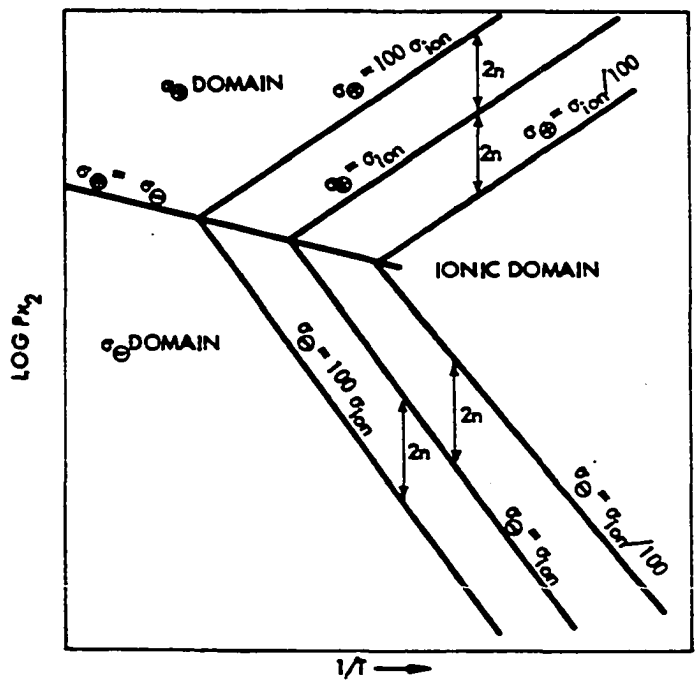

Figure 3. Relationship between electrolytic and ionic domain boundaries in Log P_{X_2}, 1/T plane

where P_{np} is the P_{X_2} at which $\sigma_{\oplus} = \sigma_{\ominus}$. Figure 2 is a schematic illustration of the variations of σ_{ion}, $\sigma_{\oplus}$ and $\sigma_{\ominus}$ for a solid electrolyte in Log σ, Log P_{X_2}, 1/T space after Patterson (46,47).

Equations [11], [12] and [13] plot as straight lines in Log P_{X_2}, 1/T space. Thus as indicated in Figure 3 the triangular region bounded by Equations [11] and [12] is called the ionic conductivity domain or simply the ionic domain (46,47). Similarly the regions bounded by Equations [11] and [13] and Equations [12] and [13] are called the hole domain and the excess electronic domain respectively. Also shown in Figure 3 is the electrolytic domain as defined by Equation [7]. To be in accordance with previously established conventions, the P_{X_2} values, corresponding to any proposed solid electrolyte application, must lie within the electrolytic domain for the electrolyte in question. Therefore it is important to establish quantitatively the Log $P_{\oplus}$ and Log $P_{\ominus}$ vs. 1/T boundaries for any solid electrolyte being considered for a given application. Delineation of these Log P_{O_2}, 1/T domain boundaries for undoped thoria is one of the major objectives of the present study.

Previous Studies on Undoped Thoria

Conductivity studies

Pure thoria has a CaF_2-type crystal structure (48,49) and may be doped with various cations like Ca, Y, La etc. to produce vacancies in the oxygen sublattice. A number of these highly defective thorium oxide solid solutions have been studied by previous investigators (7,15,40,43, 48-59) with a view to elucidate their defect structures and transport

properties. Due to the prevalence of anion vacancies the major charge carriers in these oxides are oxygen ions. The electronic charge carriers (excess electrons and holes) are relatively minor and in many cases practically insignificant over a wide range of oxygen partial pressure. Many of these doped oxides are used as oxygen-ion conducting solid electrolytes--the most common being 15 mole % yttria doped thoria ($Y_{0.15}\ Th_{0.85}\ O_{1.925}$) commonly referred to as YDT. Because thoria may be easily doped to form relatively good ionic conductors, the electrical and electro-chemical properties of undoped thoria have also been investigated by Lasker and Rapp (43), Bauerle (57) and more recently by Bransky and Tallan (60,61).

The electrical conductivity of thoria has also been investigated by a number of other authors (62-70), however these studies were conducted for purposes not closely related to the present investigation. In particular, these investigations (62-70) were conducted under conditions where the thermodynamic state of thoria was ill defined. In order to properly define the state of ThO_2 for conductivity studies, it is necessary to control the total external pressure, the temperature and the oxygen chemical potential with which the ThO_2 is equilibrated. In all these investigations (62-70) the external pressure (which is nominally at 1 atm) and the temperature were reported; however, the importance of controlling P_{O_2} was completely ignored. Hence these studies (62-70) have little pertinence to the present investigation and only the more well defined conductivity studies (43,57,60,61) on undoped thoria need to be discussed in the present context.

Lasker and Rapp (43) and Bauerle (57) observed that the ionic conductivity of thoria is P_{O_2} - independent and that the p-type conductivity is proportional to $P_{O_2}^{1/4}$. These observations are consistent with the defect model for thoria, proposed initially by Lasker and Rapp (43), which assumes a relatively large abundance of anti-Frenkel defects in the undoped thoria. According to Lasker and Rapp (43); (a) these defects may be intrinsic--i.e. there are equally large numbers of oxygen interstitials and vacancies in pure thoria, or (b) "undoped" thoria may contain inadvertently added dopants which are compensated by large numbers of anionic defects. The theory, elucidating the P_{O_2} dependence of the hole and ionic conductivity in thoria, is given in Appendix A-2. The theory predicts a $P_{O_2}^{-1/4}$ dependence for n-type conductivity. It may be noted that the $\pm$ 1/4 exponent of P_{O_2} for $\sigma_{\oplus}$ and $\sigma_{\ominus}$ comply with the relation $n = 2|Z_2|$. Bransky and Tallan (60,61) observed an apparent $P_{O_2}^{1/5}$ dependence of the p-type conductivity--which could be rationalized on the basis of vacancies in the thorium sublattice as the predominant defects in thoria. However, they pointed out that a better treatment of their data results in a $P_{O_2}^{1/4}$ dependence in accordance with the defect model proposed by Lasker and Rapp (43).

The n-type conduction branch, which is expected to occur only at very low P_{O_2} was not detected by Lasker and Rapp (43) and Bauerle (57). Bransky and Tallan (60,61) detected it to a limited extent only at very high temperature (around 1600°C). Thus the conduction domains of undoped thoria especially under reducing conditions have not been completely determined.

Investigations related to conductivity

From Appendix A-1 it is apparent that the rational scaling (oxidation) rate constant of thorium may be evaluated at any temperature from the knowledge of the functional dependences of the ionic and electronic conductivity on temperature and oxygen partial pressure. In other words, one only needs to know the conduction domains, σ^{o}_{ion}, n and Q_{ion} to predict the scaling rate of thorium; because the magnitudes of σ_3 and $(\sigma_1 + \sigma_2 + \sigma_3)$ may be obtained from Equations [8 through 12]. Equation [A-1.39] in Appendix A-1 gives the expression for the rational scaling rate constant in terms of σ_{ion}, $P_{\oplus}$, and P_{θ} and n. Gerds and Mallett (71) and Levesque and Cubicciotti (72) have measured the parabolic oxidation rate of thorium in oxygen at 1 atm. from 850° to 1450° and 250° to 350°C by thermogravimetric techniques. No previous attempts to correlate the conductivity data of thoria with the directly measured scaling rate constant of thorium metal are known.

The oxygen permeability of closed end thoria tubes between 1100° to 2050°C has been determined by Smith et al. (73). In their experiments, the oxygen partial pressure at the outside was fixed by C, CO equilibrium. The total pressure of a pure oxygen atmosphere on the inside was varied. However, the authors reported their data for inside oxygen pressure of 25 microns. If the oxygen permeability through thoria is not rate limited by surface reaction, it should be possible to correlate the conductivity properties of thoria with the permeability under the assumptions that there is negligible transport of molecular or atomic oxygen through thoria. The permeation rate is then simply given by Equation [A-1.35] or Equation

[A-1.36] in Appendix A-1; with μ'_{O_2} and μ''_{O_2} corresponding to the μ_{O_2} prevailing at the two sides of the thoria tube. Thus it is possible to correlate the permeability data of Smith et al. (73) with conductivity data.

Another check on the conductivity data results from the temperature dependence of electronic conduction and the band gap energy of thoria. The band gap energy of ionic solids like thoria is approximately twice the activation energy of σ_{np} (the total electronic conductivity at p to n transition point) as shown by Heyne and Beekmans (74). Combining Equations [9], [10] and [13] the expression for σ_{np} is given by

$$\sigma_{np} = 2\ (\sigma_{\oplus}^{o}\ \sigma_{\theta}^{o})^{1/2}\ e^{-\ (Q_{\oplus} + Q_{\theta})/2RT} \qquad [14]$$

Therefore the band gap energy is simply given by $(Q_{\oplus} + Q_{\theta})$. It is apparent from Equations [11] and [12] that the band gap energy may be readily evaluated if Q_{ion} is known and if the conduction domains for thoria are properly delineated in a Log P_{O_2}, 1/T diagram. The band gap energy of thoria, estimated from optical measurements, is around 5 to 5.6 eV (75,76). From the limited observation of the n-type conduction at 1600°C, Bransky and Tallan (60) estimated the band gap energy of around 5 eV.

Statement of Purpose

The purpose of the present study is to investigate the mixed conduction properties of undoped thoria with a view to delineate its conduction domains and to correlate these properties with: (1) the scaling rate constant of thorium metal, (2) the oxygen permeability of thoria, and (3) the band gap energy of thoria.

EXPERIMENTAL APPARATUS AND METHODS

Basically three types of measurements were involved in this study. These are: (1) A.C. conductivity measurements on undoped thoria, (2) Open circuit emf measurements on undoped thoria, and (3) Scaling (oxidation) rate measurements of thorium metal.

Apparatus for A.C. Conductivity and Open Circuit Emf Measurements

The apparatus used for atmosphere and temperature control was the same for all measurements involving undoped thoria. The cell holder and furnace tube are schematically illustrated in Figure 4. The cell assembly (B) consisting of electrodes and sample in proper sequence, was held in excellent electrical contact by means of spring pressure exerted on an alumina plunger (A). Platinum electrical lead wires (C) were brought out of the furnace tube through the brass flange (E). Stupakoff type seals, (Part No. 95.2039, Latronics Corporation, Latrobe, Pa.) (D) ensured leak-tight, electrical insulation between the lead wires and the brass flange. The lead wires were further protected inside the furnace tube with individual alumina insulating tubes. The temperature of the cell was monitored by a Pt-Pt, 10% Rh thermocouple the tip of which was located as close to the cell as possible. Compensating lead wires were used to connect the thermocouple to a Joseph Kay Company Ice Point Reference System, which maintained the cold junction temperature effectively at $0^{o}C$. The output from the cold junction was connected to terminals of a plug-board. All other lead wires were directly connected to properly assigned terminals of the plug-board. The plug-board was located close to a bank of

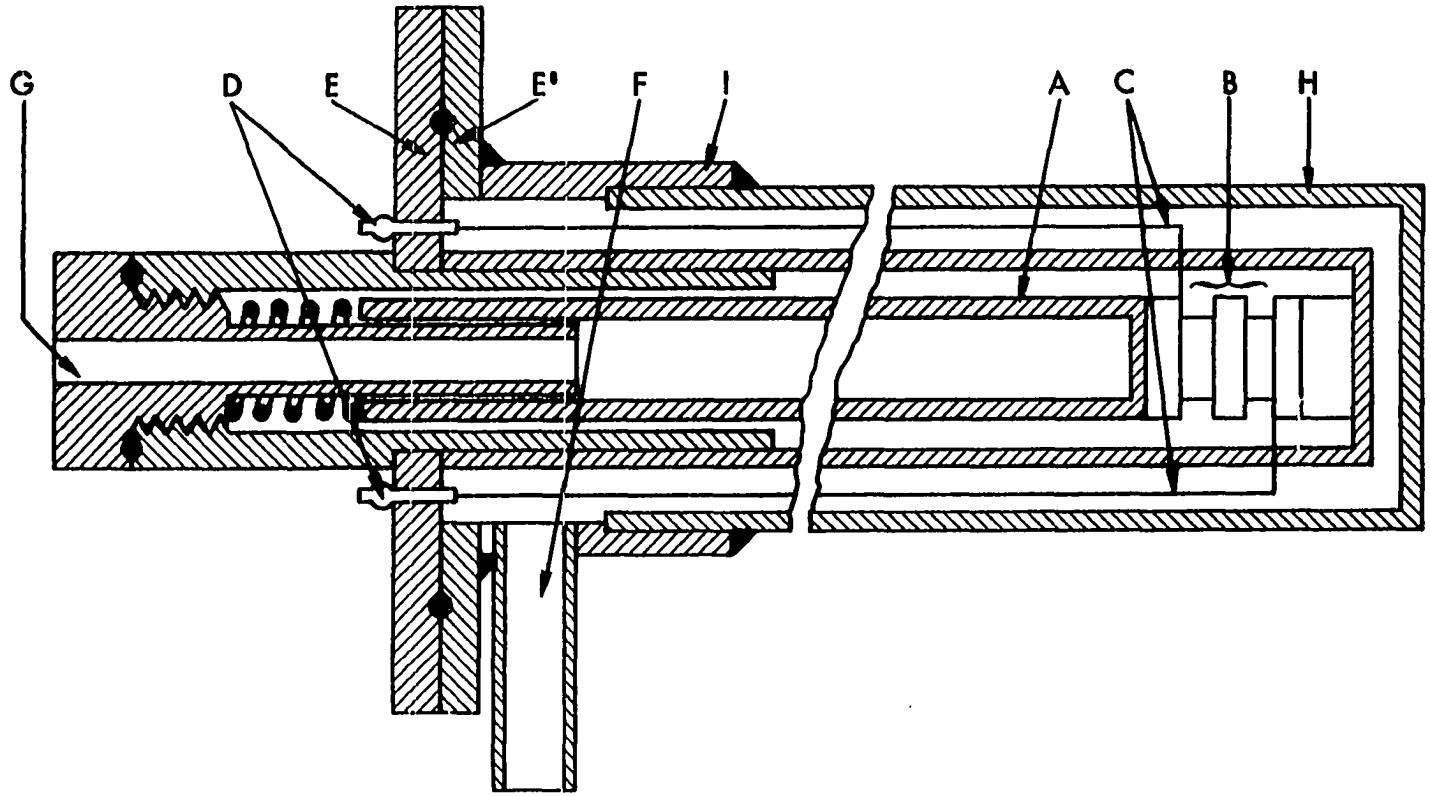

Figure 4. Design of the furnace tube and cell holder used in a.c. conductivity and open circuit emf studies

measuring instruments which facilitated a great degree of interchangeability between the different types of instruments. Shielded copper cables were used for electrical connections external to the furnace. The furnace tube (H) was also enclosed by a grounded stainless steel sheath. The shieldings of all shielded cables were also properly grounded. The open end of the furnace tube was sealed with Apiezon wax to a water cooled brass sleeve (I). The brass flange (E') was silver soldered to the brass sleeve. The flanges E and E' could be bolted together by means of six nuts and bolts (not shown in the Figure). The O-ring seal between the flanges ensured vacuum tight fit. The port F is connected to a fore-pump diffusion pump system. Port F also served as an inlet for various gases inside the furnace. Port G was used as an outlet of the gases flowing inside the furnace tube. The incoming gas inside the furnace tube was helium in most experiments. However, various $He-O_2$ and $CO-CO_2$ gas mixtures were also used in certain experiments. The gases, in these cases were mixed in a previously calibrated Matheson gas proportionator.

The heating system consisted of a silicon carbide globar furnace with the furnace tube horizontal. A chromel-alumel control couple located at the hot zone of the furnace was used in conjunction with a Leeds & Northrup Electromax Controller to regulate the cell temperature.

A Wayne Kerr Model 221 Universal Bridge operating at 1592 Hz was used for a.c. conductivity measurements. The cell temperature was monitored with a L & N 8687-1 Potentiometer and L & N 8834 d.c. Null Detector. The open circuit emfs were measured with one of the two instruments: (1) Keithley 610B Electrometer (input impedance 10^{14} Ohms) or (2) Systron

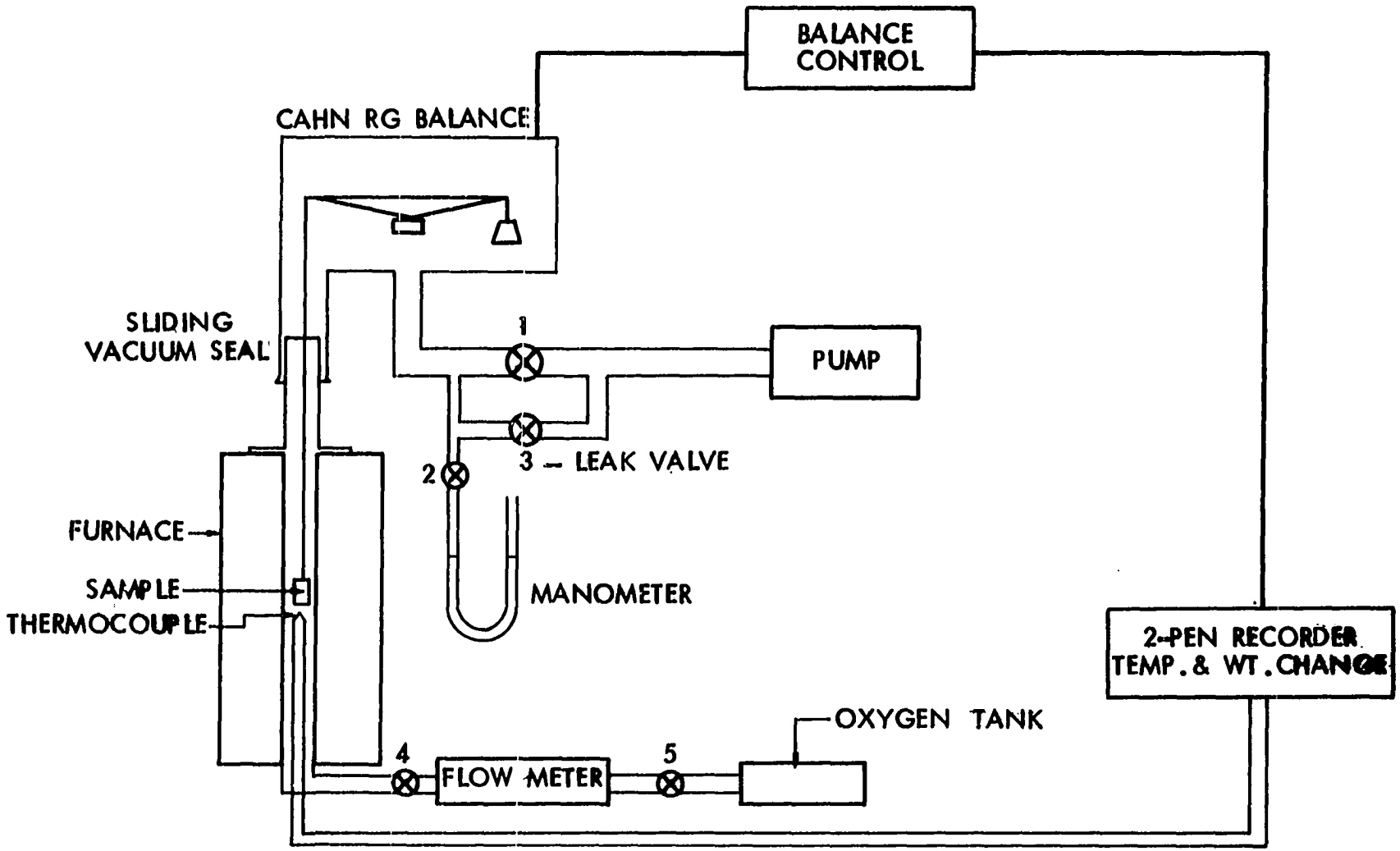

Figure 5. Schematic representation of the apparatus used in oxidation study

Donner Model 7050 Multimeter (input impedance = 10^{12} Ohms).

Apparatus For Scaling Rate Measurements

A schematic line diagram of the apparatus is given in Figure 5. The molybdnum wound resistance furnace could be raised and lowered by counter-weights and pulley mechanisms. The ground glass sliding vacuum seal enabled the sample to be held at relatively low temperature while the furnace was being heated to the desired temperature. The Cahn RG Electro-balance was used to monitor the weight change of the oxidizing sample. The Pt-Pt 10% Rh thermocouple was located in the hot zone of the furnace. The length of the platinum wire, suspending the sample from the balance, was adjusted so that the sample would be located at the hot zone when the furnace was raised. A Honeywell Elektronik 194 2 pen recorder was used to record the temperature and the weight change of the sample versus time.

Materials

Two batches of undoped thoria specimens were received from Zirconium Corporation of America. The specimens were in the form of tablets--the nominal dimensions of the first batch specimens were 3/4" diameter x 1/8" thick and that of the second batch were 1/2" diameter x 1/16" thick. The bulk density of the samples were 91 to 93% of the theoretical density. The spectrographic analysis of thoria, supplied by Zirconium Corporation of America, is reported in Table 1.

Electropolished thorium specimens were received from Metallurgy Group VII, Ames Laboratory, U. S. A. E. C., Ames, Iowa. The nominal dimensions

Table 1. Spectrographic analysis of thoria

Impurities	Wt. %
Al	0.003
Sb	N.D.
As	N.D.
Ba	N.D.
Be	N.D.
B	N.D.
Cd	N.D.
Ca	0.01
Cr	0.001
Co	0.008
Cu	0.001
Fe	0.0003
Pb	N.D.
Mg	0.0001
Mn	< 0.0001
Mo	< 0.0001
Ni	0.008
P	N.D.
Si	0.01
Ag	< 0.0001
Sr	N.D.
Sn	N.D.
Ti	N.D.
V	N.D.
Zn	N.D.
Zr	0.02
Total impurities	0.0622

of the specimens were 1 cm x 0.5 cm x 0.1 cm. Although chemical analysis of the particular batch of thorium metal is not available, Table 2 lists the major metallic impurities of a representative batch of thorium prepared by Metallurgy Group VII. The overall oxygen content (100 ppm) of the thorium specimens was higher than the limits of solubility at or below 1100°C (77).

Table 2. List of impurities in thorium metal

Impurities	ppm
La	< 0.2
Ce	< 0.2
Pr	< 0.2
Nd	< 0.6
Sm	< 0.6
Eu	< 0.6
Gd	< 0.7
Tb	< 0.2
Dy	< 0.7
Er	< 0.7
Tm	< 0.3
Yb	< 0.7
Lu	< 0.3
W	50
Re	10

A.C. Conductivity Measurements

Two probe a.c. conductivity measurements were conducted with both batches of thoria specimens. Two methods of controlling the oxygen chemical potential of the sample were used; namely, the coexistence electrode method and the controlled atmosphere method (10).

For the coexistence electrode method, identical metal, metal oxide electrodes were pressed against the two flat faces of the sample. In this method electrodes serve the dual purpose of electrical contact and of fixing the P_{O_2} at the electrode/specimen interface. The bulk of the specimen eventually becomes equilibrated with the interfacial P_{O_2} as may be shown by holding the system at the temperature of measurement until the specimen conductance reaches a steady value. In practice, however, equilibrating at the maximum temperature first greatly reduces equilibration times required at the lower temperatures and this approach was employed throughout the present study. The equilibration time varied from 1 hour to 24 hours depending on the electrode. The equilibration was more difficult to achieve with electrodes fixing low P_{O_2}. In fact in all a.c. conductivity runs involving Ti, TiO electrodes complete equilibration was never realized because excessive deterioration caused the leads to break prior to complete equilibration.

Binary mixtures of Cu, Cu_2O; Co, CoO; Ni, NiO; Mn, MnO; Nb, NbO and Ti, TiO were used as electrodes. The Mn, MnO electrode was used only for the first batch specimens because of excessive vaporization of Mn. The equilibrium P_{O_2} fixed by each electrode was calculated from the

tabulated data of the free energy of formation of the oxides (78).

The coexistence electrodes were pressed in a die from the mixtures of metal and metal oxide. The diameters of the pressed electrodes were 3/4" for the first batch specimens and 1/2" for the second batch. The dimensions of each specimen were carefully measured with a micrometer prior to each a.c. conductivity run. Care was taken to align the specimen and the electrodes properly in the cell assembly, to minimize error in the computed length to area ratio of the sample.

The controlled atmosphere method was also used in this investigation to control the P_{O_2}. In the present study this consisted of using a controlled mixture of flowing gases. Different flow ratios of CO/CO_2 and He/O_2 were passed through the system via the gas proportionator. The equilibrium P_{O_2} values fixed by CO/CO_2 mixtures were calculated using Wicks and Block's tabulations (78). Liquid platinum paint (Engelhard Industries Inc., No. 232) was applied on both the flat surfaces of the specimens, dried and fired in air at 950° to 1000°C. Repeating the process three times resulted in the formation of electrodes at the specimen surfaces, with maximum resistance of less than 0.5 ohm between point contacts on any particular electrode surface. The coated platinum electrodes were further backed up by gold foils which were connected to platinum leads of the system.

The system was evacuated to diffusion pump vacuum at the beginning of all a.c. conductivity runs and outgassed in vacuum till the temperature reached around 200°C. Helium (when metal, metal oxide electrodes were used) or the proper gas mixture (in case of platinum electrodes) was

introduced into the system and a slow steady flow of the gas was maintained during the run. The furnace was then allowed to heat up to the measuring temperatures. The equivalent parallel capacitance and conductance of the cell were measured with the Wayne Kerr bridge. After the cell equilibrated at the highest measuring temperature, conductance measurements were made while cooling and again heating up. In all cases, sufficient time was allowed for the cell to equilibrate with respect to oxygen chemical potential and temperature prior to recording the conductance values. Any difference between conductance values for heating and cooling indicated that the cell had not completely equilibrated with the desired P_{O_2} --and in those cases the temperature was cycled up and down until reproducible conductivity values were attained. All a.c. conductivity data are tabulated in Appendix B-1. The characters A and B after a particular run number indicate that the experiment was conducted with two specimens in the order: M, MO/Thoria$_A$/M, MO/M, MO/Thoria$_B$/M, Mo.

Open Circuit Emf Measurements

Equation [A-1.40] in Appendix A-1 gives the simplified expression for the open circuit emf in terms of $P_{\oplus}$, $P_{\ominus}$ and n. It is apparent that if two of these parameters are known the third one may be calculated from the observed emf and the values of P'_{O_2} and P''_{O_2} fixed at the two faces of the electrolyte. The values of $P_{\oplus}$ and n could be calculated with a reasonable degree of certainty from the a.c. conductivity measurements.

Open circuit emfs on both batches of thoria were measured with Nb, NbO and Ti, TiO electrodes. Because these electrodes fix values of Log P'_{O_2}

and Log P'_{O_2} slightly below and above the value of Log P_θ (estimated from a.c. conductivity measurements), the measured emf values give an accurate estimate of P_θ. This is because the formula, Equation [A-1.40], for the emf is a sensitive function of P_θ when P'_{X_2} and P''_{X_2} are both close to P_θ.

The method for evacuating, outgassing and filling up the system with flowing helium were similar to those of a.c. conductivity measurements. The cells were first equilibrated at the highest measuring temperature and then open circuit emfs were recorded as the cell was cooled and heated up through a series of preselected temperatures. Sufficient time was allowed for the cell to equilibrate at each temperature before a reading was recorded. The open circuit emf was monitored by the Keithley 610B Electrometer or the Systron Donner Model 7050 Multimeter. Occasionally the L & N 8687-1 Potentiometer was used with a Keithley 153 Microvoltammeter to record the emf by null balance. The emf values were found to be independent of the instruments employed.

The experiments had to be stopped by occasional lead breakage. All open circuit emf data from various runs are compiled in Appendix B-2.

Scaling Rate Measurements

The dimensions of the sample to be oxidized were carefully measured by a micrometer. It was then suspended to the balance by platinum wire. By adjusting the balance control the initial counterpoise load was matched with the weight of the sample. The system was evacuated with the valves Nos. 2 and 4 (Figure 5) closed. The furnace, kept in its lowest position,

was allowed to heat up to the temperature. The change in weight of the sample and the temperature of the furnace were monitored continuously by the Honeywell Elektronik 194 recorder. No detectable increase in weight of the sample was observed during the heating up period of the furnace. The furnace was raised to the highest level after the temperature was stabilized at the desired value. Oxygen was immediately admitted by opening valves Nos. 4 and 5 and closing valves No. 1, 2, and 3 (see Figure 5). A steady flow of oxygen was maintained by opening valve No. 3. The oxygen pressure inside the system was maintained and monitored close to one atmosphere by opening valve No. 2 and adjusting the leak valve No. 3 so that the oil in both arms of the manometer was kept at the same level.

The scaling rate experiments were conducted for four temperatures viz. 800°, 900°, 1000° and 1100°C.

The weight increases of the thorium samples are tabulated vs. $\sqrt{t}$ where t is in minutes in Appendix B-3.

RESULTS AND DISCUSSION

Electrical Conductivity of Thoria

Arrhenius type behavior was observed for the electrical conductivity data of every run tabulated in Appendix B-1. Figures 6 and 7 show the 1100°, 1000°, 900° and 800°C isotherms of Log σ versus Log P_{O_2} for first and second batch thoria specimens. The data points shown in the figures were obtained by extrapolation or interpolation of the linear Log σ versus 1/T plots. The P_{O_2} independent ionic conductivity (plateau) of thoria is evident from the horizontal segments of the conductivity isotherms.

Figure 8 illustrates the Arrhenius type behavior of the ionic conductivity for both batches of thoria. Figure 8 also includes the ionic conductivity data for thoria generated from the minima of the total conductivity isotherms, reported by Lasker and Rapp (43). Bauerle's (57) 1000°C data for the ionic conductivity fall right on the Lasker-Rapp ionic conductivity line. The P_{O_2}-independent ionic conductivities may be expressed as

$$\text{Log } \sigma_{ion} \text{ (Batch 1)} = 1.94 - 44357/4.575T \qquad [15]$$

$$\text{Log } \sigma_{ion} \text{ (Batch 2)} = 1.69 - 41550/4.575T \qquad [16]$$

$$\text{Log } \sigma_{ion} \text{ (Lasker \& Rapp)} = 1.30 - 34000/4.575T \qquad [17]$$

Bransky and Tallan (60,61) reported conductance isotherms, instead of conductivity isotherms. The activation energy for ionic conduction, estimated from the minima of their conductance isotherms, is approximately 23400 calories/mole.

The larger magnitude of ionic conductivity observed by Lasker and Rapp

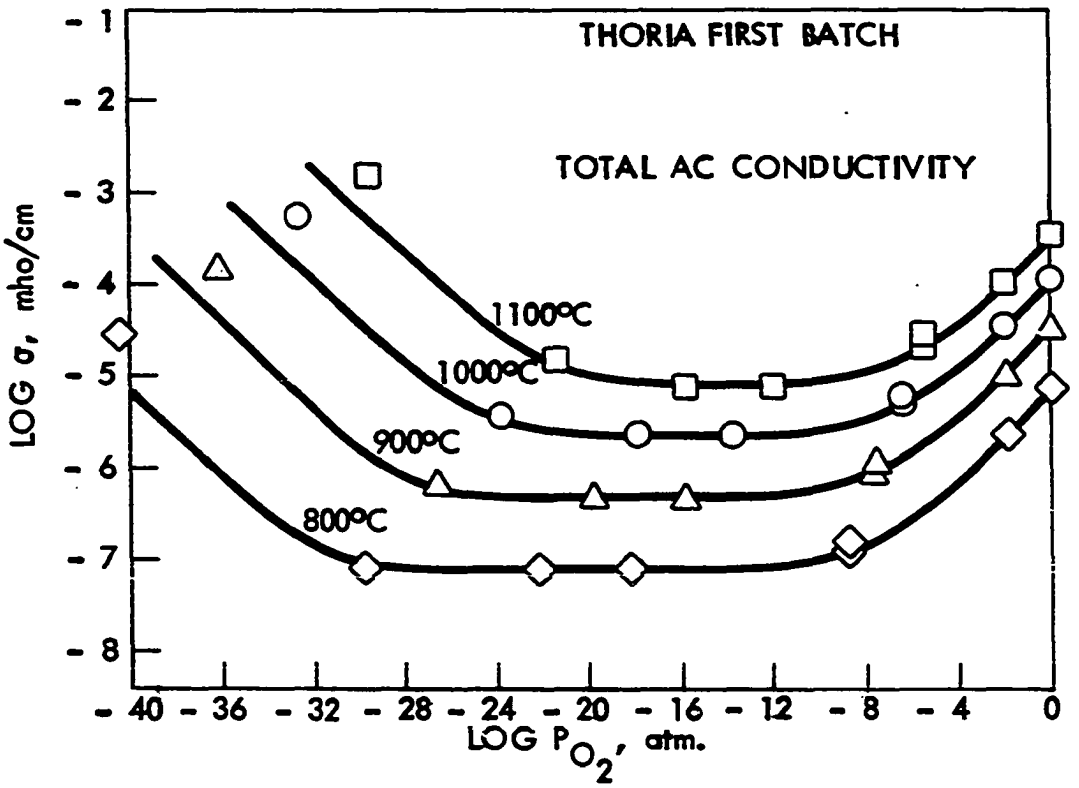

Figure 6. Log σ_{total} versus Log P_{O_2} isotherms for 1st batch thoria specimens

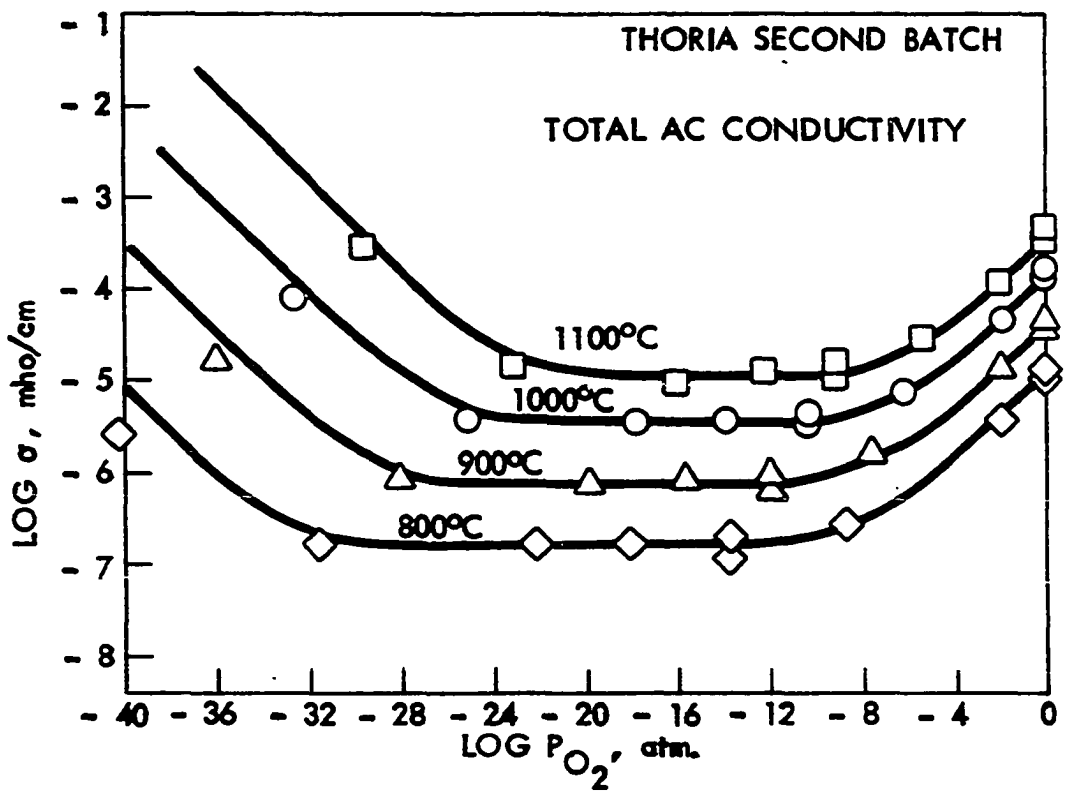

Figure 7. Log σ_{total} versus Log P_{O_2} isotherms for 2nd batch thoria specimens

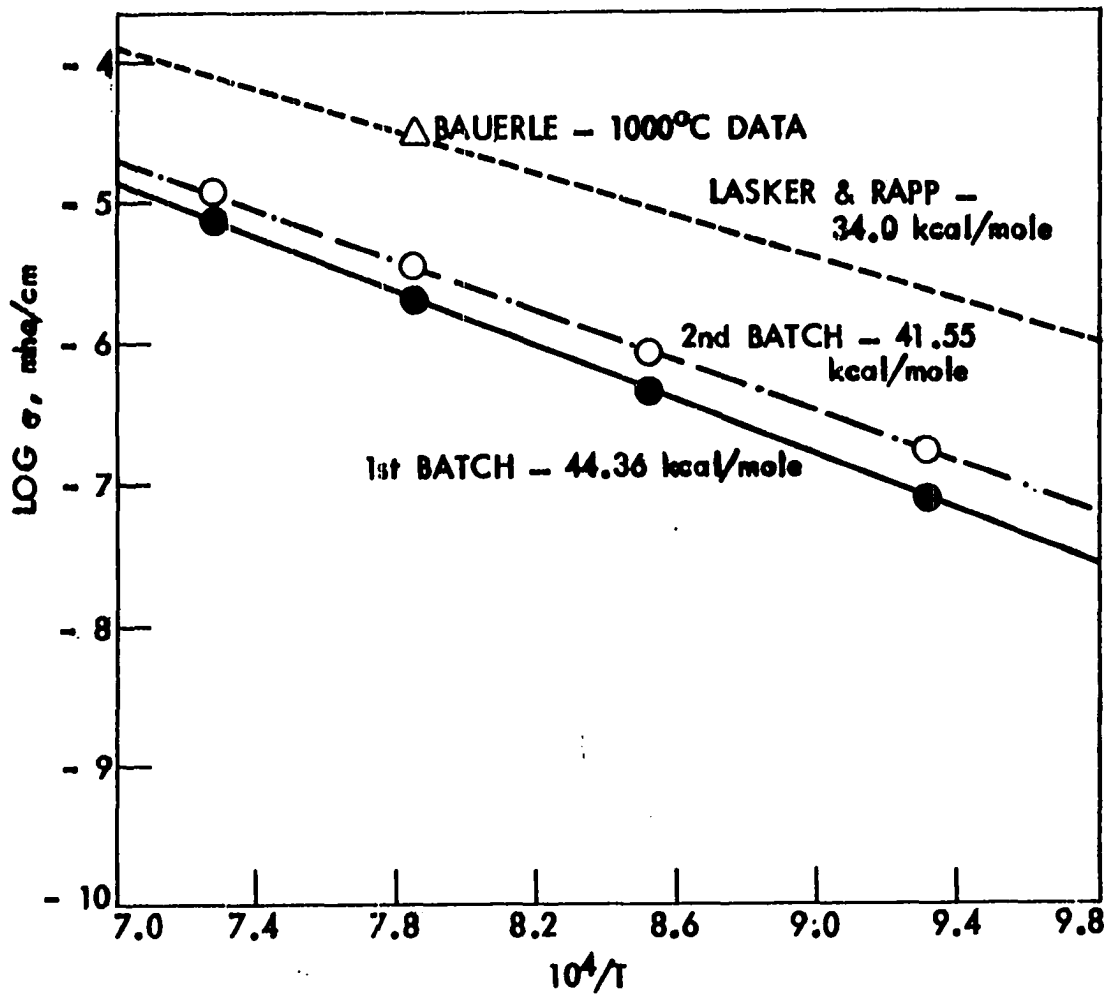

Figure 8. Log σ versus $10^4/T$ plots for the ionic conductivity of thoria

(43) may be possibly due to higher dopant (inadvertently added) level in the thoria specimens used in their investigation. In view of the higher ionic conductivity of the 2nd batch specimens compared to that of the 1st batch, it is likely that the 2nd batch thoria contains more dopant than the 1st batch thoria even though the impurity contents (reported by the supplier) of both batches are the same. The activation energies for ionic conduction for 1st batch, 2nd batch and Lasker and Rapp's thoria are 44.36, 41.55 and 34.00 kcals/mole--this trend of decreasing activation energy also suggests increasing dopant level in accordance with the assumption that the temperature range (1100° to 800°C), of the present investigation and of Lasker and Rapp, is within the transition region between impurity (dopant) controlled and intrinsic ionic conduction. Under such circumstances a curvature is expected to be observed in the Arrhenius plot, however, preliminary graphical constructions* indicate that the curvatures are expected to be substantially less than the scatter in the experimental conductivity data.

The p-type conduction branch is quite well delineated in the conductivity isotherms of Figures 6 and 7. The procedure to determine n,

---

* $\sigma_{ion} = A\, e^{-Q_1/RT} + B\, e^{-Q_2/RT}$ was the equation assumed for the variation of the ionic conductivity in the transition region. The value of Q_1 (the activation energy for intrinsic conduction) was chosen to be 60 kcals/mole and that of Q_2 (the activation energy for impurity controlled ionic conduction) to be 30 kcals/mole. By proper manipulation of the constants A and B, it could be shown that the deviation from linearity of the Arrhenius plot was less than 0.1 in Log σ for the apparent activation energy of 45 kcals/mole (or less), within the temperature range of 800° to 1100°C. Further quantitative calculations were not pursued because the magnitudes of Q_1 and Q_2 are not known.

where $P_{O_2}^{1/n}$ characterizes the P_{O_2} dependence of the p-type conduction branch is detailed below.

The function Log $[1 + (P_{O_2}/P_{\oplus})^{1/n}]$ was plotted versus Log $(P_{O_2}/P_{\oplus})$ in a translucent graph paper for values of n = 3, 4 and 5. For low values of $(P_{O_2}/P_{\oplus})$ the function plots as a horizontal straight line with the ordinate value effectively equal to zero. This horizontal part will be referred to as the "base-line." The translucent graph paper was laid over the data points of a particular conductivity isotherm so that the base line coincided with the horizontal portion (the ionic conductivity plateau) of the isotherm. By lateral shifting of the graph paper (while maintaining the plateau and the base line in coincidence), the best fits for the data points with the loci of the function Log $[1 + (P_{O_2}/P_{\oplus})^{1/n}]$ were obtained for n = 3, 4 and 5. This is illustrated in Figure 9 for the 1100°C conductivity isotherm of 2nd batch thoria specimens. It is apparent from Figure 9 that the overall best fit is obtained for n = 4. In all the conductivity isotherms illustrated in Figures 6 and 7 the best fit was obtained for the value of n = 4, in accordance with previous investigations (43, 57, 60, 61). Thus at high Log P_{O_2} values the solid lines for the conductivity isotherms indicate the best-fits of the data points obtained by the above procedure with n = 4. The value of Log $P_{\oplus}$ at a particular temperature is the Log P_{O_2} value which coincides with Log $(P_{O_2}/P_{\oplus})$ = 0 of the translucent graph at the position of best fit. The Log $P_{\oplus}$ values ranged from -6 to -7.4 (for 1st batch) and from -5.9 to -7.6 (for 2nd batch) for the temperature range 1100° to 800°C. The Log $P_{\oplus}$ values (for 800°, 900°, 1000° and 1100°C) may be plotted against 1/T as straight lines (Figures 10 and 11)

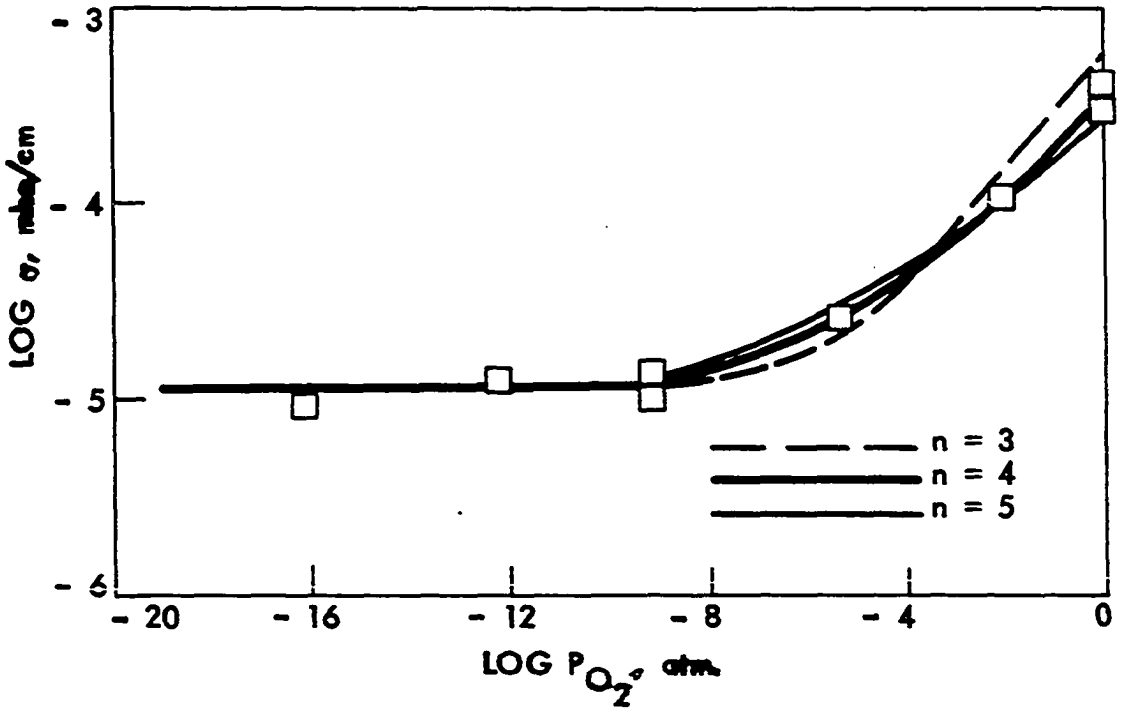

Figure 9. High P_{O_2} region of the 1100°C conductivity isotherm of 2nd batch thoria showing the best fit for $P_{O_2}^{1/4}$ dependence of the p-type conductivity

according to the following equations

$$\text{Log } P_{\oplus} \text{ (1st batch)} = -1.00 - 31443/4.575\ T \qquad [18]$$

$$\text{Log } P_{\oplus} \text{ (2nd batch)} = 0.63 - 40427/4.575\ T \qquad [19]$$

where, according to Equation [11], 31443 cals/mole and 40427 cals/mole represent $4\ (Q_{ion} - Q_{\oplus})$ for the 1st and 2nd batch thoria specimens.

Although an accurate determination of Log $P_{\oplus}$ is not possible from the conductivity isotherms reported by Lasker and Rapp (43), Bauerle (57) and Bransky and Tallan (60,61); a reasonable estimate indicates that the values of Log $P_{\oplus}$ are between -5 and -8 (in all the investigations) for the temperature range 800° to 1100°C. The estimated value of Log $P_{\oplus}$, from the conductivity isotherms of Lasker and Rapp (43), is around -5 with little or no observable dependence on temperature.

The low P_{O_2} conductivity runs with Ti, TiO electrodes were not successful, although a major part of the effort was directed toward this end. In all cases the equilibration times were excessively long and the runs had to be stopped due to lead breakage prior to complete equilibration. Bransky and Tallan (60,61) also experienced difficulties due to lead breakage at low P_{O_2} in their investigations. Tallan and Vest (41) reported similar problems at low P_{O_2} in their investigations with yttria. In view of the difficulties, a.c. conductivity runs with Ti, TiO electrodes (Runs No. 10* and No. 22), in the present study, can only be interpreted

---

*It may be noted that the 1st batch thoria specimen, used in Run No. 10, was prereduced by heating it up to 1200°C in contact with thorium metal.

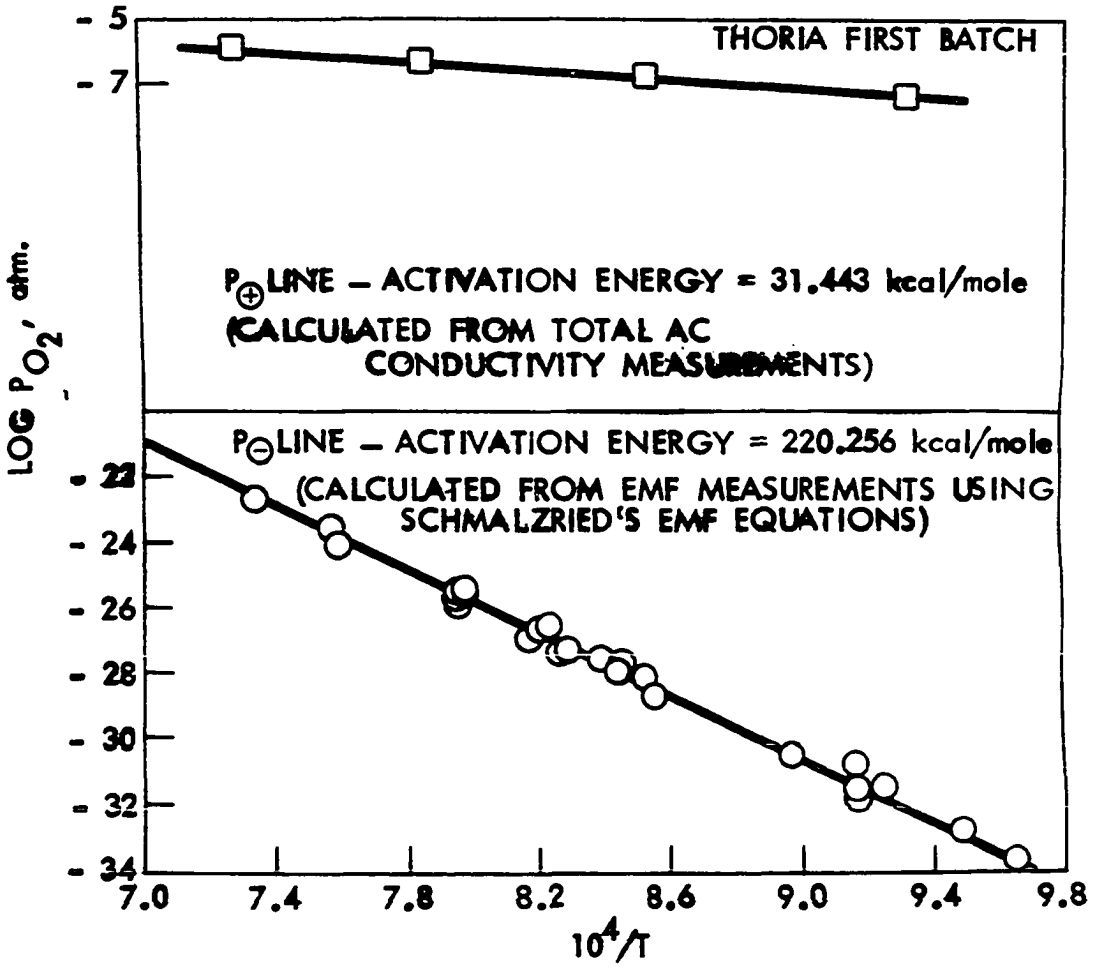

Figure 10. Log $P_{\ominus}$ and Log $P_{\oplus}$ versus $10^4/T$ for 1st batch thoria

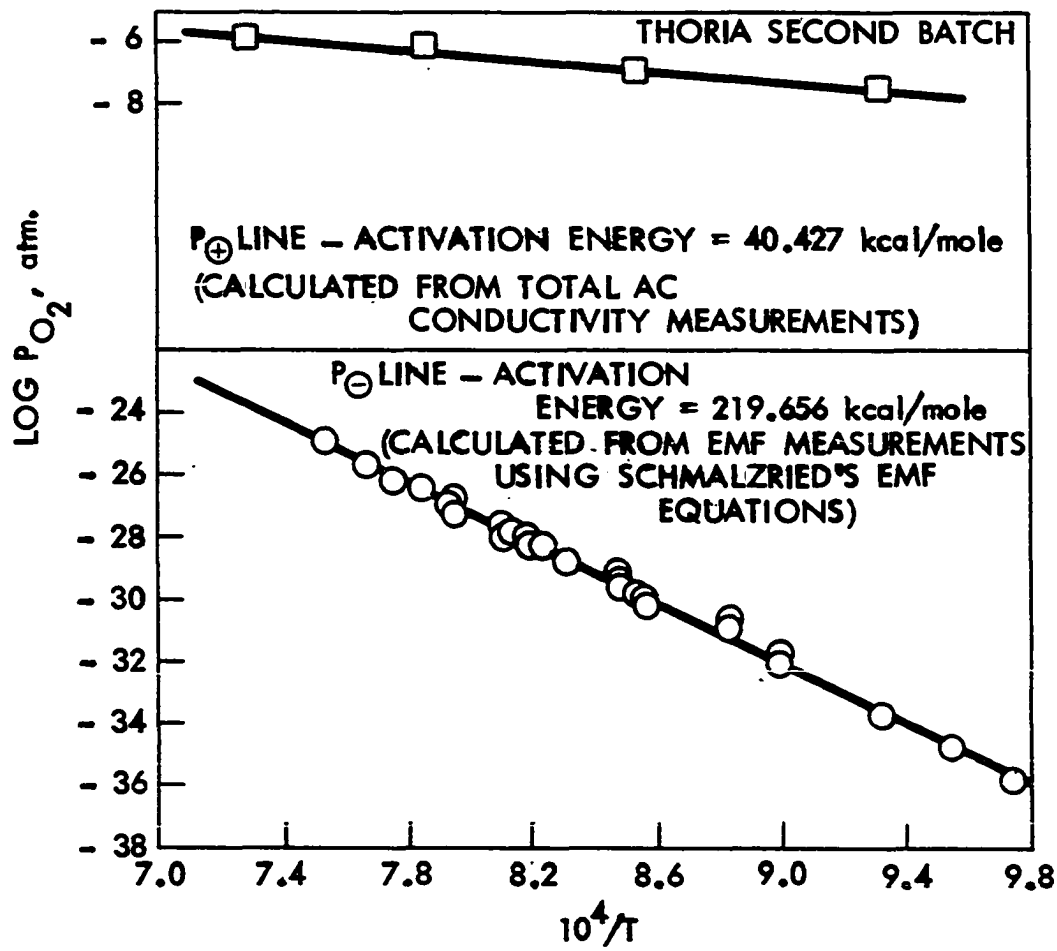

Figure 11. Log $P_\ominus$ and Log $P_\oplus$ versus $10^4/T$ for 2nd batch thoria

qualitatively. The elevated* a.c. conductivity values show that excess electronic conductivity is substantially greater than the partial ionic conductivity at these low P_{O_2} values. However, lead breakage problems precluded the possibility of obtaining precise data for these conditions. It may be concluded from these runs that P_θ for undoped thoria lies substantially above coexistence P_{O_2} values for Ti, TiO equilibrium. This prediction was confirmed by open circuit emf measurements, discussed below.

Determination of P_θ: Open Circuit Emf Measurements

Open circuit emf measurements were made to determine the P_θ of thoria. When $P_\oplus$ is very large compared to the P_θ, Schmalzried's formula, Equation [A-1.40] in Appendix A-1, suggests that open circuit emf will be a sensitive function of P_θ for P'_{O_2} and P''_{O_2} close to P_θ. Under such conditions, the effect of slight variation in the value of $P_\oplus$ causes an imperceptible variation on the open circuit emf. In other words, the P_θ may be determined, almost independently of the $P_\oplus$, from the observed emf. Equation [A-1.40] assumes that the value of n characterizing the P_{X_2} dependences of the p-type and the n-type conduction is the same for both the conduction branches (i.e. the p-type and the n-type branches). This assumption requires further discussion and justification.

Bransky and Tallan (60) estimated the value of n = 6 for the n-type conduction branch from their limited observations at low P_{O_2}. On the

---

*The possibility of the increase in a.c. conductivity due to doping by titanium was considered. Electron microprobe analyses showed no perceptible contamination of the specimen by Ti, TiO electrodes.

other hand, they are in accord, with Lasker and Rapp (43), Bauerle (57) and the present investigation, on the value of n = 4 for the p-type conduction branch. The difference in the values of n for the two conduction branches is apparently inconsistent with the defect model (Appendix A-2) proposed by Lasker and Rapp (43) and corroborated further by Bauerle (57) and Bransky and Tallan (60,61). In view of Equation [A-2.8] the concentration of excess electrons may, perhaps, exhibit $P_{O_2}^{-1/6}$ dependence only at extremely low P_{O_2}, at which the oxygen vacancy concentration is no longer constant but is dictated by the excess electron concentration. In fact, under such conditions the oxygen vacancy concentration is half of the excess electron concentration. However, the most important premise, on which the accepted defect model of thoria is based, is that there exists a wide range of P_{O_2} in which the oxygen defect (vacancies and interstitials) concentrations are virtually constant. The $P_{O_2}^{1/4}$ dependence of the p-type conduction branch is a direct outcome of this consideration. Therefore, according to Equation [A-2.10] there should exist an intermediate P_{O_2} range (with constant oxygen defect concentration) in which the n-type conductivity would exhibit a $P_{O_2}^{-1/4}$ dependence. Therefore, the $P_{O_2}^{-1/4}$ dependence for n-type conductivity is justified and used in the interpretation of the low P_{O_2} open circuit emf data.

Ti, TiO and Nb, NbO electrodes were chosen to fix the P'_{O_2} and P''_{O_2} values at the opposite faces of the thoria specimens, used for the low P_{O_2} open circuit emf studies. The choice was based on the value of P_θ roughly estimated from the a.c. conductivity measurements involving Ti, TiO coexistence electrodes. The open-circuit emf runs also suffered due to

lead breakage resulting from the extremely reducing conditions. Appendix B-2 lists the data compiled for all the open circuit emf runs. The scatter in the data prevented attempts to obtain any meaningful correlation between observed emf and temperature. However, Log P_θ values calculated from the data plotted linearly versus 1/T with a scatter band well within one order of magnitude (Figures 10 and 11). A Fortran computer program (listed in Appendix C-1) was used to obtain the least-square best-fit equation of the Log P_θ versus 1/T from emf data. The resulting equations may be expressed as

$$\text{Log } P_\theta \text{ (1st batch)} = 12.68 - 220256/4.575T \qquad [20]$$

$$\text{Log } P_\theta \text{ (2nd batch)} = 11.23 - 219656/4.575T \qquad [21]$$

The possibility, of niobium or titanium doping by diffusion from the electrodes, was considered. Electron microprobe traces, through a few thoria samples used in open circuit emf measurements, indicated no discernible titanium or niobium penetration.

The low P_{O_2} parts of the solid lines in the conductivity isotherms (Figures 6 and 7) were generated on the basis of the Log P_θ values, obtained from emf measurements.

Activation Energy Determinations for p-Type and n-Type Conduction

According to Equation [11] the slope of the Log $P_\oplus$ vs. 1/T line gives n $(Q_{ion} - Q_\oplus)$. Therefore,

$$Q_\oplus = Q_{ion} - Q_{P_\oplus}/n \qquad [22]$$

where the energy term $Q_{P_\oplus}$ is deduced from the slope of Log $P_\oplus$ vs. 1/T.

The activation energies for both batches of thoria for p-type conduction, calculated from the above equation are 36496 cals/mole (1st batch) and 31425 cals/mole (2nd batch).

Similarly the temperature dependence of P_θ and Equation [12] leads to

$$Q_\theta = Q_{ion} + Q_{P_\theta}/n \qquad [23]$$

where Q_{P_θ} is deduced from the slope of the low P_{O_2} ionic domain boundary, given by Equation [20] or Equation [21].

The activation energies Q_θ for n-type conduction, calculated from Equation [23] are 99420 cals/mole (1st batch) and 96464 cals/mole (2nd batch).

According to Equation [14], the band gap energy is given by $(Q_\oplus + Q_\theta)$. Hence the experimentally determined values of $Q_\oplus$ and Q_θ yield band gap energies of 5.89 eV and 5.54 eV for the specimens of batch 1 and batch 2, respectively. These values compare favorably with 5.0 to 5.6 eV estimated from optical measurements (75, 76) and independent conductively measurements (60).

The Electrolytic Domain of Thoria

It is apparent from Equation [7], that a mixed conductor may be used as a solid electrolyte at a particular temperature if the difference between Log $P_\oplus$ and Log P_θ is at least 4 n. Thus for thoria this difference must be at least 16 Log units at the temperature in question. This leads to rather limited ranges of electrolytic domain at 1100°C of 0.4 (between -14 and -14.4 in Log P_{O_2}) for the 1st batch and of 1.7 (between -13.9 and -15.6 in Log P_{O_2}) for the 2nd batch. Dropping to 800°C widens the

electrolytic domains to 8.7 (between -15.4 and -24.1 in Log P_{O_2}) for 1st batch and to 9.9 (between -15.6 to -25.5 in Log P_{O_2}) for the 2nd batch. Although the electrolytic domain is expected to become broader at lower temperature, the successful use of undoped thoria as a solid electrolyte is doubtful because of its prohibitively high resistance.

Lasker and Rapp (43) postulated that the n-type conductivity line (see Figure 1) moves to lower P_{O_2} values with the addition of dopants which increase the ionic conductivity by introducing oxygen ion vacancies. It is apparent from Figure 1 that the value of Log P_θ (which is at the point of intersection of the n-type and the ionic conductivity lines) will move to lower Log P_{O_2} values just by increasing the magnitude of ionic conductivity, while keeping the n-type conductivity line fixed. However, if the n-type conductivity line also moves to lower P_{O_2} values, the Log P_θ will move even farther in this same direction. Qualitatively this trend is observed between the two batches of thoria. Thus, for example, at 1000°C one would predict, for fixed n-type conductivity line of 1st batch, an approximate value of Log P_θ = -25.8 for the 2nd batch. This is the Log P_{O_2} value at which the n-type conductivity of 1st batch is equal to the ionic of 2nd batch at 1000°C. However, the value, from open circuit emf measurements, is found to be -26.4 (Figure 11).

According to Lasker and Rapp (43) the magnitude of Log σ_{ion} at 1000°C for 15 mole % yttria doped thoria is -2.1. The predicted value of Log P_θ of 15% yttria doped thoria, on the basis of fixed n-type conductivity line of 1at batch, is around -39.2 at 1000°C. However, Tretyakov and Muan (40) and Hardaway et al. (59) estimated the value of Log P_θ at 1000°C for 15

mole % yttria doped thoria to be -30.6 and -30.0. Thus, the n-type conductivity line appears to move to higher P_{O_2} value in 15 mole % yttria doped thoria. This is contrary to Lasker and Rapp's prediction (43).

Oxygen Permeability of Thoria

The Fortran computer program listed in Appendix C-2 was used to determine oxygen permeability of thoria tubes on the basis of Equations [A-1.36] and [A-1.39] (Appendix A-1). Input information provided to the program includes the value of n = 4 as well as the Arrhenius temperature dependences of σ_{ion}, P'_{O_2}, P''_{O_2}, $P_{\oplus}$ and $P_{\ominus}$. By using experimentally determined temperature dependences of σ_{ion}, $P_{\oplus}$ and $P_{\ominus}$, the oxygen permeability of undoped thoria tubes was calculated for P'_{O_2}, P''_{O_2} and T values where permeability measurements have been made.

Smith, Meszaros and Amata (73) have reported oxygen permeability data of thoria tubes for an inside oxygen pressure of 25 microns, outside oxygen partial pressure presumably corresponding to C, CO equilibrium and for temperatures ranging from 1100° to 2050°C. For comparison the oxygen permeability for both batches of thoria was calculated with P''_{O_2} equal to 25 microns and with P''_{O_2} calculated from tabulated free energy data for C, CO equilibrium (78).

In addition to calculations for 1st and 2nd batch thoria of the present study, the oxygen permeability was also calculated for the thoria used in the investigation by Lasker and Rapp (43) with σ_{ion} calculated according to Equation [17]. The value of Log $P_{\oplus}$ was assumed to be -5 and independent of temperature. Because no $P_{\ominus}$ data is available from Lasker and Rapp's

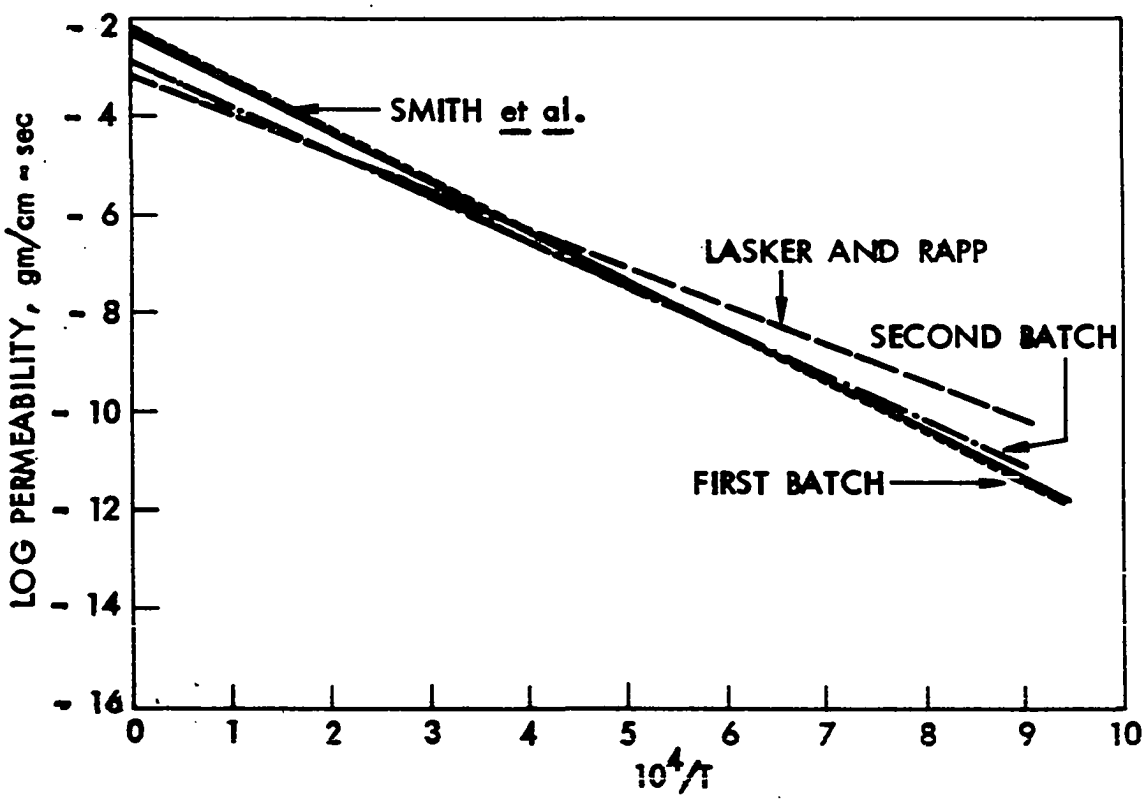

Figure 12. Log oxygen permeability versus $10^4/T$ plots for thoria

investigation, the Log P_θ for the 2nd batch, given by Equation [21] was used for the calculation.

The directly measured permeability of Smith et al. (73) may be expressed in gms/cm sec as

$$\text{Log Permeability (Smith et al.)} = -2.33 - 46100/4.575T \quad [24]$$

whereas the calculated permeabilities in gms/cm sec may be listed as follows:

$$\text{Log Permeability (1st batch)} = -2.25 - 46356/4.575T \quad [25]$$

$$\text{Log Permeability (2nd batch)} = -2.77 - 42150/4.575T \quad [26]$$

$$\text{Log Permeability (Lasker and Rapp)} = -3.15 - 35463/4.575T \quad [27]$$

Figure 12 compares the calculated temperature dependences of the oxygen permeability with the measurements reported by Smith et al. (73) shown as the solid line. The agreement between the measured and calculated permeability, especially for the 1st batch thoria specimens (dotted line), is noteworthy. Significantly, the thoria specimens for this investigation and the thoria tubes used for the permeability measurements were supplied by the same manufacturers, namely, the Zirconium Corporation of America.

Scaling (Oxidation) Rate Constant of Thorium

Figure 13 is a plot of Log k vs. $10^4/T$, where k is the rational oxidation constant of thorium in moles/cm sec for an ambient oxygen pressure of 1 atm. Gerds and Mallett reported an activation energy of 62800 cals/mole for their scaling rate measurements which were made in the temperature range 850° to 1450°C (71). Levesque and Cubicciotti (72) obtained an activation energy of 31000 cals/mole from their low temperature (250° to

to 350°C) measurements.

These measurements may be compared with the calculated values of the rational scaling rate constant for thorium metal. The calculations were made with the computer program listed in Appendix C-2, which is the same program for oxygen permeability calculations. However, in this case the value P''_{O_2} was set equal to 1 atm. and the value of P'_{O_2} was calculated from tabulated data (78) for Th, ThO_2 equilibrium coexistence. The values of n, $P_{\oplus}$, $P_{\ominus}$ and σ_{ion} were the same as of batches 1 and 2 of this study and mentioned earlier in connection with the oxygen permeability calculations. The calculated rational scaling rate constants may be expressed as follows:

$$\text{Log } k \text{ (1st batch)} = -3.42 - 44866/4.575T \qquad [28]$$

$$\text{Log } k \text{ (2nd batch)} = -3.76 - 41695/4.575T \qquad [29]$$

$$\text{Log } k \text{ (Lasker \& Rapp)} = -4.16 - 34280/4.575T \qquad [30]$$

These calculations are compared with the known scaling rate constant measurements for thorium metal in Figure 13. The disagreement between the various calculated and measured rational scaling rate constants prompted the present investigator to conduct thermogravimetric oxidation study of thorium at 800°, 900°, 1000° and 1100°C. When plotted as weight gain versus the square root of time, the data for each run listed in Appendix B-3 exhibited the expected linear behavior with the usual deviations from linearity observed at very short times. Similar short-time deviations have been observed and discussed by many other investigators, notab'y by Wagner and Grünewald (79) in connection with the investigation of the

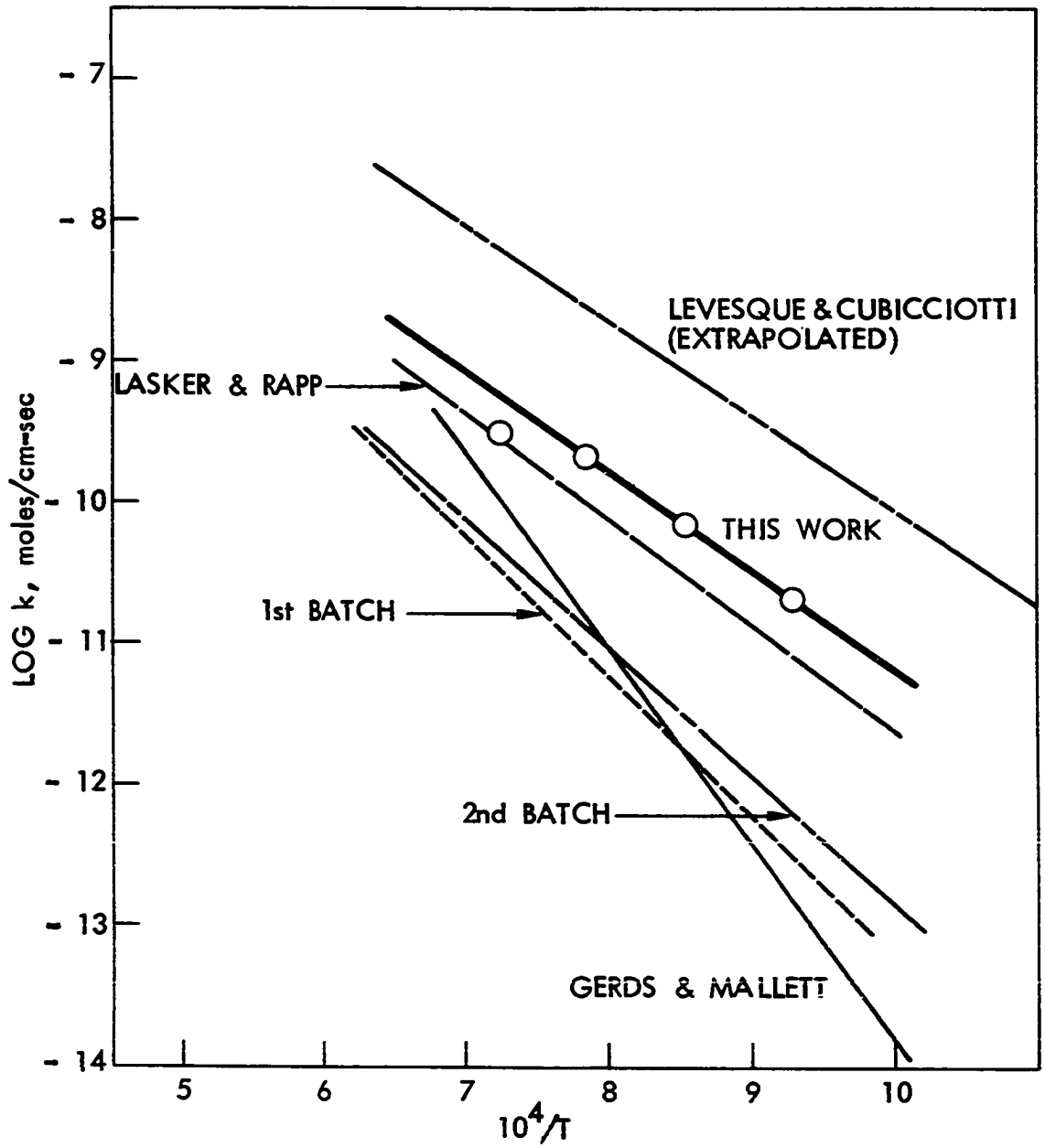

Figure 13. Log k (rational scaling rate constant) versus $10^4/T$ plots for thorium metal oxidizing in pure oxygen at 1 atm.

oxidation kinetics of copper.

The practical scaling rate constant (k') in $gm^2/cm^4 sec$ was calculated directly from the slope of the linear part of the weight gain versus $\sqrt{t}$ plot and then converted to the rational scaling rate constant (k) in moles/cm sec by using the equation

$$k = 1/32\ \bar{V}\ \left(\frac{|Z_2|}{A_X}\right)^2\ k' \qquad [31]$$

In Equation [31] $\bar{V}$ is the molar volume of thoria in c.c./mole, Z_2 the valency of oxygen and A_X the atomic weight of oxygen. Equation [31] is equivalent to Equation [4.10] given by Hauffe (80), except for a factor of 1/16. This factor enters because k is calculated in moles/cm sec and $\bar{V}$ is the molar volume in Equation [31], whereas k is in equivalent/cm sec and $\bar{V}$ is the equivalent volume in Hauffe's Equation [4.10].

The rational scaling rate constants, measured in the present study, are shown as circles in Figure 13. In the temperature range 800° to 1000°C, the results of these measurements yield

$$\text{Log } k = -4.29 - 31260/4.575T \qquad [32]$$

as the temperature dependence of the rational scaling rate constant.

As shown in Figure 13, the scaling rate measurements made in this study fall intermediate between the two previously reported studies (71,72) with the slope in the 800° to 1000°C range matching quite closely to the slope observed by Levesque and Cubicciotti (72) at low temperatures.

It is apparent from Figure 13 that the predictions of the oxidation

rate of thorium from conductivity data, emf data and Equation [A-1.39] were not successful as were the permeability predictions discussed earlier. Presumably a substantial amount of study regarding the nature of the oxide scales on thorium metal would be required to explain the discrepancies between calculated and measured value for the scaling rates of thorium metal in oxygen. Such matters, for example, as heat liberation, the P_{O_2} dependence of the rate constant, and scale morphology, state of stress, and purity would be very helpful in resolving the discrepancies. Such investigations lie beyond the intended scope of the present study. These investigations might also be helpful in determining whether or not there is significance to the relatively close agreement between the thorium oxidation rate measurements of the present investigation and the values calculated from Equation [A-1.39] with the conductivity data of Lasker and Rapp (43) (and with Equation [21] for P_θ).

CONCLUSIONS

1. Mixed conduction in thoria at elevated temperatures may be characterized in terms of a P_{O_2} independent ionic conductivity, a p-type conductivity proportional to $P_{O_2}^{1/4}$ and a n-type conductivity proportional to $P_{O_2}^{-1/4}$.

2. For a given batch of thoria there exist well-defined conditions, i.e. Log P_{O_2} - 1/T domains, wherein ionic conductivity, n-type conductivity and p-type conductivity each predominate--these are designated respectively as the ionic, the excess electron and positive hole domains.

3. Thoria exhibits predominant n-type conduction under reducing conditions at elevated temperatures.

4. The various conductivity domains of thoria are separated by well-defined straight lines on a Log P_{O_2} - 1/T diagram; however, the precise location and slope of these boundaries vary perceptibly for different batches of as-purchased, undoped thoria.

5. Undoped thoria exhibits a very limited electrolytic domain ($t_{ion} > 0.99$) between 800° and 1100°C.

6. The permeability of crack-free thoria tubes to oxygen gas may be predicted quantitatively as a function of temperature from the temperature and P_{O_2} dependences of the partial ionic and electronic conductivities of thoria used to make the tubes.

7. The oxidation kinetics of thorium metal in pure oxygen gas at 1 atm pressure are parabolic with a rational scaling rate constant k exhibiting the following Arrhenius temperature dependence in the range 800° to $1000^{\circ}C$:

$$\text{Log } k = -4.29 - 31260/4.575T$$

8. The use of Wagner's theory of oxidation with conductivity parameters determined from as-purchased, undoped thoria predicts rational scaling rate constants for thorium metal oxidation which are not in quantitative agreement with measured values.

9. The band gap energy for thoria is estimated from the temperature dependence of n-type and p-type conduction. This yields a value from 5.5 to 5.9 eV at elevated temperatures, in reasonable agreement with the value of 5.0 to 5.6 eV estimated from optical measurements.

LITERATURE CITED

1. D. A. MacInnes, "The Principles of Electrochemistry," Dover Publications, New York, N.Y., 1961, pp. 20.

2. W. Nernst, Z. Electrochemie 6 (2), 41 (1899).

3. J. Frenkel, Z. Physik 35, 652 (1926).

4. C. Wagner and W. Schottky, Z. Phys. Chemie (B) 11, 163 (1930).

5. C. Wagner, Z. Phys. Chemie 21 (1-2), 25 (1933).

6. K. Kiukkola and C. Wagner, J. Electrochem. Soc. 104 (5), 308 (1957).

7. K. Kiukkola and C. Wagner, J. Electrochem. Soc. 104 (5), 379 (1957).

8. C. B. Alcock, Ed., "Electromotive Force Measurements in High-Temperature Systems," American Elsevier Publishing Company, Inc., New York, N.Y., 1968.

9. D. O. Raleigh in "Progress in Solid State Chemistry," H. Reiss, Ed., Pergamon Press, New York, N.Y., Vol. 3, pp. 83-134.

10. R. A. Rapp and D. A. Shores in "Physicochemical Measurements in Metals Research," R. A. Rapp Ed., in Techniques of Metals Research, R. F. Bunshah, Series Ed., Interscience Publishers, New York, N.Y. 1970, Vol. 4, Part 2, pp. 123-192.

11. J. D. Schieltz, "Electrolytic Behavior of Yttria and Yttria Stabilized Hafnia," Unpublished Ph.D. thesis. Ames, Iowa, Library, Iowa State University, 1970.

12. R. A. Rapp, Trans. Met. Soc. A.I.M.E., 227 (4), 371 (1963).

13. C. B. Alcock and S. Zador, Electrochimica Acta, 12 (6), 673 (1967).

14. S. Ignatowicz and M. W. Davies, J. Less Common Metals 15, 100 (1968).

15. B. C. H. Steele and C. B. Alcock, Trans Met. Soc. A.I.M.E. 233 (7), 1359 (1965).

16. R. N. Blumenthal, J. B. Moser and D. H. Whitmore, J. Amer. Ceram. Soc. 48 (12) 617, (1965).

17. H. Schmalzried, Z. Phys. Chemie, N. F. 25 (3/4), 178 (1960).

18. L. D. Yushina, S. F. Pal'guev and S. V. Karpachev, Zhur. Fiz. Khim 35, 342 (1961).

19. W. H. Skelton, N. J. Magnani and J. F. Smith, Met. Trans. 2 (2), 473 (1971).

20. A. Kubik and C. B. Alcock in "Electromotive Force Measurements in High-temperature Systems," C. B. Alcock Ed., American Elsevier Publishing Company, Inc., New York, N.Y. 1968, pp. 43-49.

21. L. R. Bidwell and R. Speiser, Acta Met. 13 (2), 61 (1965).

22. R. J. Fruehan, L. J. Martonik and E. T. Turkdogan, Trans. Met. Soc. A.I.M.E. 245 (7), 1501 (1969).

23. K. Schwerdtfeger, Trans. Met. Soc. A.I.M.E. 239 (9), 1276 (1967).

24. G. R. Fitterer, C. D. Cassler and V. L. Vierbicky, J. Metals 21 (8), 46 (1969).

25. J. Weissbart and R. Ruka, Rev. Scientific Instruments 32 (5), 593 (1961).

26. L. G. Austin, "Fuel Cells," National Aeronautics and Space Administration Report NASA SP-120, Washington, D.C., 1967.

27. M. N. Hull, Energy Conversion 10, 215 (1970).

28. J. Weissbart and R. Ruka, J. Electrochem. Soc. 109 (8), 723 (1962).

29. D. H. Archer, E. F. Sverdrup and R. L. Zahradnik, Chem. Eng. Progr. 60, 64 (1964).

30. R. L. Pastorek and R. A. Rapp, Trans. Met. Soc. A.I.M.E. 245, 1711 (1969).

31. H. Rickert and A. A. ElMiligy, Z. Metallk 59, 635 (1968).

32. H. Rickert, H. Wagner and R. Steiner, Chem. Ing. Tech. 38, 618 (1966).

33. H. Rickert and R. Steiner, Z. Physik Chem. N.F. 62, 119 (1968).

34. D. O. Raleigh and H. R. Crowe, J. Electrochem. Soc. 116, 40 (1969).

35. D. O. Raleigh, J. Electrochem. Soc. 114 493, (1967).

36. K. B. Oldham and D. O. Raleigh, J. Electrochem. Soc. 118, 252 (1971).

37. H. Rickert in "Electromotive Force Measurements in High-temperature Systems," C. B. Alcock, Ed., American Elsevier Publishing Company Inc., New York, N.Y., 1968, pp. 59-90.

38. V. B. Tare and H. Schmalzried, Trans. Met. Soc. A.I.M.E. 236, 444 (1966).

39. D. Yuan and F. A. Kröger, J. Electrochem. Soc. 116, 594 (1969).

40. Y. D. Tretyakov and A. Muan, J. Electrochem. Soc. 116, 311 (1969).

41. N. M. Tallan and R. W. Vest, J. Amer. Ceram. Soc. 49 (8), 401 (1966).

42. F. A. Kröger and H. J. Vink in "Solid State Physics," F. Seitz and D. Turnbull Eds., Academic Press, New York, N.Y., 1956, Vol. 3, pp. 307-435.

43. M. F. Lasker and R. A. Rapp, Z. Physik Chem. N.F. 49, 198 (1966).

44. H. Schmalzried, Z. Elektrochem. 66, 572 (1962).

45. H. Schmalzried, Z. Phys. Chem. N.F. 38, 87 (1963).

46. J. W. Patterson in "The Physics of Electronic Ceramics," L. L. Hench and D. B. Dove Eds., Marcel Dekker Inc., New York, N.Y., in press.

47. J. W. Patterson, to be published in J. Electrochem. Soc.

48. F. Hund, Ber. dtsch. Keram. Ges 42, 251 (1965).

49. D. M. Roy and R. Roy, J. Electrochem. Soc. 111, 421 (1964).

50. F. Hund and W. Durrwachter, Z. Anorg. Allg. Chem. 265, 67 (1951).

51. F. Hund and R. Mezger, Z. Physik. Chem. 201, 268 (1952).

52. E. C. Subbarao, P. H. Sutter and J. Hrizo, J. Amer. Ceram. Soc. 48, 443 (1965).

53. F. Hund, Z. Anorg. Allg. Chem. 274, 105 (1953).

54. J. Rudolph, Z. Naturforsch A14, 727 (1959).

55. J. M. Wimmer, L. R. Bidwell and N. M. Tallan, J. Amer. Ceram. Soc. 50, 198 (1967).

56. A. A. Vecher and D. V. Vecher, Russian J. Phys. Chem. (English Translation) 4, 685 (1967).

57. J. E. Bauerle, J. Chem. Phys. 45, 4162 (1966).

58. J. W. Patterson, E. C. Bogren and R. A. Rapp, J. Electrochem. Soc. 114, 752 (1967).

59. J. B. Hardaway III, J. W. Patterson, D. R. Wilder and J. D. Schieltz, J. Amer. Ceram. Soc. 54 (2), 94 (1971).

60. I. Bransky and N. M. Tallan, J. Amer. Ceram. Soc. 53, 625 (1970).

61. N. M. Tallan and I. Bransky, J. Electrochem. Soc. 118, 345 (1971).

62. J. L. Bates, BNWL-473, Battelle Northwest Laboratories, Richland, Washington, 1967.

63. J. L. Bates, BNWL-CC-821, Battelle Northwest Laboratories, Richland, Washington, 1966.

64. W. E. Danforth and J. H. Bodine, J. Franklin Inst. 260, 467 (1955).

65. W. E. Danforth, J. Chem. Phys. 23 591 (1955).

66. G. Mesnard and R. Uzan, Le Vide 6, 1052 (1951).

67. G. Mesnard and R. Uzan, Le Vide 6, 1091 (1951).

68. G. Mesnard, Comptes Rendus 232, 1744 (1951).

69. W. E. Danforth and F. H. Morgan, Phys. Rev. 79, 142 (1950).

70. M. Foex, Comptes Rendus 215, 534 (1942).

71. A. F. Gerds and M. W. Mallett, J. Electrochem. Soc. 101, 171 (1954).

72. P. Levesque and D. Cubicciotti, J. Amer. Chem. Soc. 73, 2028 (1951).

73. A. W. Smith, F. W. Meszaros and C. D. Amata, J. Amer. Ceram. Soc. 49, 240 (1966).

74. L. Heyne and N. M. Beekmans, "Electronic Transport in Calcia Stabilized Zirconia," British Ceramic Society Meeting on Mass Transport in Non-Metallic Solids, London, December 17-18, 1969.

75. O. A. Weinreich and W. E. Danforth, Phys. Rev. 88, 953 (1952).

76. R. C. Linares, J. Phys. Chem. Solids 28, 1285 (1967).

77. D. T. Peterson, Trans. Met. Soc., A.I.M.E. 221, 924 (1961).

78. C. E. Wicks and F. E. Block, "Thermodynamic Properties of 65 Elements," U.S. Bureau of Mines Bulletin 605, 1963.

79. C. Wagner and K. Grünewald, Z. Physik. Chem. (B) 40, 455 (1938).

80. K. Hauffe, "Oxidation of Metals," Plenum Press, New York, N.Y., 1965, pp. 147.

APPENDICES

The appendices appear in the following pages (60 to 93). Appendix A-1 and Appendix A-2 are concerned with the theory. Appendices B-1, B-2 and B-3 list the experimental data. The computer programs, used in this investigation, appear in Appendix C-1 and Appendix C-2.

APPENDIX A-1. SUMMARY OF WAGNER'S THEORY OF MIXED CONDUCTION

Consider a virtually stoichiometric ionic compound $M_a X_b$. For simplicity let us restrict to linear flux geometry i.e. consider the $M_a X_b$ specimen of uniform cross section and let the partial pressures of X_2 gas at the two opposite faces be P'_{X_2} (atm.) and P''_{X_2} (atm.). The chemical potentials in (calories/mole) at these two faces are then given by

$$\mu'_{X_2} = \mu^{o}_{X_2} + RT \ln P'_{X_2} \qquad [A\text{-}1.1]$$

and

$$\mu''_{X_2} = \mu^{o}_{X_2} + RT \ln P''_{X_2} \qquad [A\text{-}1.2]$$

where $\mu^{o}_{X_2}$ is the chemical potential of X_2 gas in the standard state (X_2 gas at 1 atm.), R the gas constant and T the absolute temperature.

The mobile species in the specimen are the cations (M^{Z1}), anions (X^{Z2}) and electrons e (both excess electrons and holes). The superscripts Z_1 and Z_2 are respectively the valences of the cations and anions and are given by

$$Z_i = - (q_i/q_3) \qquad [A\text{-}1.3]$$

where q_i is the charge in coulombs on a particular ion and q_3 that of an electron and subscripts 1 and 2 denote the cations and anions respectively.

Under steady-state open circuit condition the net electrical current at any location in the specimen is zero; in other words

$$\sum_{i=1}^{3} q_i J_i = 0 \qquad [A\text{-}1.4]$$

where J_i is the flux of ith species. Phenomenologically we can write J_i as the product of the concentration (c_i), absolute mobility (B_i) and the sum of the negative gradient of all pertinent potentials. In particular, two potentials need to be considered in the present case. They are the chemical potential and the electrostatic potential. These two potentials may be conveniently combined to form the electro-chemical potential η_i according to the following relation

$$\eta_i = \mu_i + \frac{q_i N \Phi}{4.186} \qquad [A-1.5]$$

where N is the Avogadro's number, Φ the electrostatic potential in volts, and μ_i and η_i have units of calories/mole.

$$\therefore J_i = - \frac{c_i B_i}{N} \nabla \eta_i \qquad [A-1.6]$$

where c_i is the concentrations in particles/c.c., B_i is the absolute mobility in cm^2/cal sec and J_i is the particle flux in particles/cm^2 sec.

in view of the relation $\sigma_i = q_i^2 c_i B_i / 4.186$ [A-1.7]

where σ_i is the electrical conductivity (mho/cm). Equations [A-1.4] and [A-1.6] may be combined to yield

$$\sum_{i=1}^{3} q_i J_i = - \sum_{i=1}^{3} \frac{4.186\ \sigma_i}{N\ q_i} \nabla \eta_i = 0 \quad . \qquad [A-1.8]$$

The following chemical equilibria are used to express η_1 and η_2 in terms of μ_{X_2}, μ_M and η_3 which may be measured and controlled in a physical system:

$$M = M^{Z1} + Z_1 e \qquad [A-1.9]$$

$$\therefore \nabla\mu_M = \nabla\eta_1 + Z_1\nabla\eta_3, \qquad [A\text{-}1.10]$$

(because the electrostatic force cannot act on a neutral particle $\nabla\eta_M = \nabla\mu_M$).

Similarly

$$X = X^{Z_2} + Z_2\, e \qquad [A\text{-}1.11]$$

and $$1/2\ \nabla\mu_{X_2} = \nabla\eta_2 + Z_2\nabla\eta_3 \qquad [A\text{-}1.12]$$

It should be noted that Z_2 is a negative quantity. Using Equations [A-1.10] and [A-1.12] in Equation [A-1.8] results in

$$-\frac{\sigma_1}{q_1}(\nabla\mu_M - Z_1\nabla\eta_3) - \frac{\sigma_2}{q_2}(1/2\ \nabla\mu_{X_2} - Z_2\nabla\eta_3) = \frac{\sigma_3}{q_3}\nabla\eta_3 \qquad [A\text{-}1.13]$$

The generalized Gibbs-Duhem relation for the $M_a X_b$ compound may be written as

$$c_1\, d\eta_1 + c_2\, d\eta_2 + c_3\, d\eta_3 = 0 \qquad [A\text{-}1.14]$$

$$\therefore\ c_1\nabla\eta_1 + c_2\nabla\eta_2 + c_3\nabla\eta_3 = 0\ . \qquad [A\text{-}1.15]$$

Using Equation [A-1.10] and Equation [A-1.12] we get

$$c_i\nabla\mu_M + 1/2\ c_2\nabla\mu_{X_2} + (c_3 - c_1Z_1 - c_2Z_2)\nabla\eta_3 = 0 \qquad [A\text{-}1.16]$$

The assumption of local charge neutrality yields

$$q_1c_1 + q_2c_2 + q_3c_3 = 0 \qquad [A\text{-}1.17]$$

Equation [A-1.3] and Equation [A-1.17] may be combined to yield

$$c_3 - c_1Z_1 - c_2Z_2 = 0 \qquad [A\text{-}1.18]$$

$\therefore$ Equation [A-1.16] reduces to

$$c_1 \nabla\mu_M + 1/2\ c_2 \nabla\mu_{X_2} = 0 \qquad \text{[A-1.19]}$$

It should be noted that in a virtually stoichiometric compound $M_a X_b$

$$\frac{c_1}{c_2} = \frac{a}{b} = -\frac{Z_2}{Z_1} = -\frac{q_2}{q_1} \qquad \text{[A-1.20]}$$

$$\therefore\ \nabla\mu_M = 1/2\ \frac{q_1}{q_2}\ \nabla\mu_{X_2} \qquad \text{[A-1.21]}$$

Equation [A-1.21] may be used to replace $\nabla\mu_M$ with $1/2\ \frac{q_1}{q_2}\ \nabla\mu_{X_2}$ and vice versa in Equation [A-1.13], which combined with Equation [A-1.3] yields

$$-\frac{(\sigma_i + \sigma_2)}{q_1}\ \nabla\mu_M = -\frac{(\sigma_1 + \sigma_2)}{2\,q_2}\ \nabla\mu_{X_2} = \frac{(\sigma_1 + \sigma_2 + \sigma_3)}{q_3}\ \nabla\eta_3 \qquad \text{[A-1.22]}$$

The ionic transference number is the sum of the ionic conductivities divided by the total conductivity. Therefore,

$$-\frac{t_{ion}}{q_1}\ \nabla\mu_M = -\frac{t_{ion}}{2q_2}\ \nabla\mu_{X_2} = \frac{\nabla\eta_3}{q_3} \qquad \text{[A-1.23]}$$

where t_{ion} is the ionic transference number.

Equation [A-1.23] may be integrated from one end of the specimen to the other to yield

$$\frac{-1}{q_1}\int_{\mu'_M}^{\mu''_M} t_{ion}\, d\mu_M = \frac{-1}{2q_2}\int_{\mu'_{X_2}}^{\mu''_{X_2}} t_{ion}\, d\mu_{X_2} = \frac{1}{q_3}\,(\eta''_3 - \eta'_3) \qquad \text{[A-1.24]}$$

where the single and double primes refer to the opposite ends of the specimen.

Assuming that the electrical leads (connected to a suitable measuring

instrument) at the opposite ends of the specimen are of the same composition and that the temperature is uniform across the specimen; the chemical potentials of the electrons (in the leads), at the opposite ends of the specimen, are virtually equal. Therefore in view of Equation [A-1.5],

$$\eta_3'' - \eta_3' = \frac{q_3 N}{4.186} \quad (\bar{\Phi}'' - \bar{\Phi}') \qquad [A\text{-}1.25]$$

Therefore Equation [A-1.24] reduces to

$$-\frac{4.186}{q_1 N} \int_{\mu_M'}^{\mu_M''} t_{ion}\, d\mu_M = -\frac{4.186}{2q_2 N} \int_{\mu_{X_2}'}^{\mu_{X_2}''} t_{ion}\, d\mu_{X_2} = (\bar{\Phi}'' - \bar{\Phi}') \qquad [A\text{-}1.26]$$

The Faraday's constant F in calories/volt equivalent is given by

$$F = -\frac{q_3 N}{4.186} \qquad [A\text{-}1.27]$$

$\therefore$ In view of Equation [A-1.3], Equation [A-1.25] reduces to

$$-\frac{1}{Z_1 F} \int_{\mu_M'}^{\mu_M''} t_{ion}\, d\mu_M = -\frac{1}{2Z_2 F} \int_{\mu_{X_2}'}^{\mu_{X_2}''} t_{ion}\, d\mu_{X_2} = (\bar{\Phi}'' - \bar{\Phi}') \qquad [A\text{-}1.28]$$

Equation [A-1.28] is the expression for the open circuit emf originally derived by Wagner (5).

Now consider the growth of a $M_a X_b$ scale on a metal M in X_2 gas. Let the chemical potentials of M and X_2 at the metal/scale interface be given by μ_M' and μ_{X_2}' and similarly at the scale/X_2 gas interface by μ_M'' and μ_{X_2}''. The rate of growth of $M_a X_b$ per unit area in molecules/sec is then given by

$$\dot{n}_{M_a X_b} = \frac{J_1}{a} - \frac{J_2}{b} \qquad [A\text{-}1.29]$$

Equations [A-1.4] and [A-1.20] may be combined to yield

$$\dot{n}_{M_a X_b} = \frac{J_1}{a} - \frac{J_2}{b} = \frac{q_3}{q_2 b} J_3 \qquad [A\text{-}1.30]$$

In view of Equations [A-1.6], [A-1.7] and [A-1.27], Equation [A-1.30] may be written as

$$\dot{n}_{M_a X_b} = \frac{\sigma_3}{q_2 b F} \nabla \eta_3 \qquad [A\text{-}1.31]$$

Replacing $\nabla \eta_3$ in favor of $\nabla \mu_{X_2}$ according to Equation [A-1.22]

$$\dot{n}_{M_a X_b} = \frac{-q_3}{2q_2^2 b F} \cdot \frac{\sigma_3 (\sigma_1 + \sigma_2)}{(\sigma_1 + \sigma_2 + \sigma_3)} \nabla \mu_{X_2} \qquad [A\text{-}1.32]$$

At a particular instant of time the rate of growth per unit area may be obtained by integrating Equation [A-1.32] over the thickness of the scale. Restricting considerations to linear geometry we get

$$\dot{n}_{M_a X_b}(t) L = - \frac{q_3}{2q_2^2 bF} \int_{\mu'_{X_2}}^{\mu''_{X_2}} \frac{\sigma_3 (\sigma_1 + \sigma_2)}{(\sigma_1 + \sigma_2 + \sigma_3)} d\mu_{X_2} = k \qquad [A\text{-}1.33]$$

where $\dot{n}(t)$ and L are the instantaneous growth rate (in molecules/sq cm sec) and scale thickness (cm) and k is the rational oxidation (scaling rate) constant in molecules/cm sec (5).

Consider the case of a $M_a X_b$ compound with the partial pressures P'_{X_2} and P''_{X_2} fixed at its two opposite sides. In this case we want to derive an expression for the permeability of X_2 gas through the $M_a X_b$ compound. Let $P''_{X_2} > P'_{X_2}$. Therefore from Equations [A-1.1], [A-1.2] and

[A-1.21] we have $\mu''_{X_2} > \mu'_{X_2}$ and $\mu''_M < \mu'_M$. Therefore in the cell $P'_{X_2}/M_a X_b/P'_{X_2}$, the flux J_1 will be from left to right and the flux J_2 from right to left. Because there is no source or sink of M ions at the two ends of the specimen, the flux J_1 can only be maintained by the following chemical equation

$$aM + 1/2\ bX_2 \rightleftharpoons M_a X_b \qquad \text{[A-1.34]}$$

where the arrow to the right indicates the reaction at right interface of the above cell and the arrow to the left indicates the reaction at the left interface. From the above considerations, a flux J_1 from left to right is equivalent to an additional flux of anion equal to $\frac{b|J_1|}{a}$ from right to left.

Therefore the net flux J_2 through the specimen is given by

$$\left(\frac{b\,J_1}{a} - J_2\right).$$

$\therefore$ From Equation [A-1.29] the net flux J_2 in particles/sq cm sec is given by $b\,\dot{n}_{M_a X_b}$.

Under the assumption of the constant thickness L of the $M_a X_b$ specimen, Equation [A-1.33] may be used to get the expression for J_2 which is given by

$$J_2 = \frac{k\,b}{L} \qquad \text{[A-1.35]}$$

The effective flux of X_2 gas in molecules/sq cm sec through the specimen is then given by

$$J_{X_2} = \frac{k\,b}{2\,L} = -\frac{q_3}{4q_2^2 LF}\int_{\mu'_{X_2}}^{\mu''_{X_2}} \frac{\sigma_3\,(\sigma_1+\sigma_2)}{(\sigma_1+\sigma_2+\sigma_3)}\,d\mu_{X_2} \qquad \text{[A-1.36]}$$

The permeability (73) or more precisely the permeation rate of X_2 gas for 1 cm thick $M_a \times_b$ specimen is, therefore, given by $\frac{kb}{2}$ (molecules/cm sec).

In the case of a predominantly ionic conductor Schmalzried (44,45) has formulated a closed-form solution for the integral

$$\int_{\mu'_{X_2}}^{\mu''_{X_2}} t_{ion}\, d\mu_{X_2}$$

appearing in Equation [A-1.28], with the assumptions that σ_{ion} = (which is the sum of σ_1 and σ_2) is P_{X_2} independent and the n-type and the p-type electronic conductivities are proportional to $P_{X_2}^{-1/n}$ and $P_{X_2}^{1/n}$ respectively. Schmalzried's solution is given below

$$\int_{\mu_{X_2'}}^{\mu_{X_2}''} t_{ion}\, d\mu_{X_2} = RT\, \frac{n}{\sqrt{\omega}} \ln \left[\frac{2(P_{X_2}/P_{\oplus})^{1/n} + 1 - \sqrt{\omega}}{2(P_{X_2}/P_{\oplus})^{1/n} + 1 + \sqrt{\omega}} \right] \Bigg|_{P'_{X_2}}^{P''_{X_2}} \qquad [A\text{-}1.37]$$

$$\text{where } \omega = 1 - 4\left[\frac{P_\theta}{P_\oplus}\right]^{1/n} \qquad [A\text{-}1.38]$$

under the above assumptions the rational scaling rate constant k, in Equation [A-1.33 or [A-1.36] has the following solution

$$k = \frac{-q_3}{2q_2^2 bF} \cdot RT\, \sigma_{ion} \left\{ \ln \frac{P''_{X_2}}{P'_{X_2}} - \frac{n}{\sqrt{\omega}} \ln \left[\frac{2(P_{X_2}/P_{\oplus})^{1/n} + 1 - \sqrt{\omega}}{2(P_{X_2}/P_{\oplus})^{1/n} + 1 + \sqrt{\omega}} \right] \Bigg|_{P'_{X_2}}^{P''_{X_2}} \right\} \qquad [A\text{-}1.39]$$

Schmalzried (44,45) has given an alternative (very slightly approximate but much less cumbersome) solution for the expression appearing in Equation [A-1.37]. Using this solution the expression for the open circuit emf reduces to

$$(\bar{\Phi}' - \bar{\Phi}') = -\frac{nRT}{2Z_2F} \cdot \left[\ln \frac{P_{\oplus}^{1/n} + P'^{1/n}_{O_2}}{P_{\oplus}^{1/n} + P'^{1/n}_{O_2}} + \ln \frac{P_{\ominus}^{1/n} + P'^{1/n}_{O_2}}{P_{\ominus}^{1/n} + P'^{1/n}_{O_2}}\right]$$

[A-1.40]

APPENDIX A-2. DEFECT MODEL AND CONDUCTIVITY OF THORIA

According to Lasker and Rapp (43) thoria contains a large number of oxygen interstitials and vacancies. These defects may be intrinsic i.e. there are approximately as many oxygen interstitials as there are vacancies. These defects may also be produced by inadvertently added cationic dopants of valency other than 4 (the valency of thorium) according to the following chemical equilibria:

$$M + V_{Th}^{-4} = M_{Th}^{(Z_M-4)} + 1/2\ (4-Z_M)\ V_O^2 \qquad [A\text{-}2.1]$$

or

$$M_e + V_{Th}^{-4} = M_{e_{Th}}^{(Z_{M_e}-4)} + 1/2\ (Z_{M_e}-4)\ O_i^{-2} \qquad [A\text{-}2.2]$$

where M and M_e are neutral metallic dopant atoms with valences Z_M (< 4) and Z_{M_e} (> 4). V_{Th}^{-4} is a vacancy in thorium sublattice which reacts with the dopants to form substitutional cations $M_{Th}^{(Z_M-4)}$ and $M_{e_{Th}}^{(Z_{M_e}-4)}$ on the thorium in sublattice. V_O^2 and O_i^{-2} are oxygen vacancies and interstitials. The superscripts indicate the effective valencies on each defect.

In either of the two possible mechanisms for the creation of defects in the oxygen sublattice it is assumed that the concentrations of the anion vacancies and/or the interstitials are high and relatively constant over a wide range of P_{O_2}. Consider the following chemical reaction

$$O_O = V_O^2 + O_O^{-2} \qquad [A\text{-}2.3]$$

where O_O is an oxygen ion in its normal site.

The equilibrium constant for the reaction is given by

$$k_3 = [V_O^2]\ [O_O^{-2}] \qquad [A\text{-}2.4]$$

where the quantities in brackets denote concentration. In view of Equation [A-2.4] it is apparent that if the concentration of one of the defects is invariant, the concentration of the other is also invariant.

The ionic conductivity is assumed to be due only to oxygen ions. Because the ionic conductivity is proportional to the lattice defect concentrations (the mobility of each defect is assumed to be concentration independent), the ionic conductivity is constant over a wide range of P_{O_2}.

The electron-holes are produced at relatively high P_{O_2} according to the following chemical equilibrium

$$1/2\ O_2\ (gas) = O_i^{-2} + 2h^1 \qquad [A\text{-}2.5]$$

where h^1 is a hole with effective valence of +1. The equilibrium constant of the reaction [A-2.5] is given by

$$k_5 = [O_i^{-2}]\ [h^1]^2\ P_{O_2}^{-1/2} \qquad [A\text{-}2.6]$$

Because $[O_i^{-2}]$ is relatively invariant over a wide range of P_{O_2}

$$[h^1] = k_5'\ P_{O_2}^{1/4} \qquad [A\text{-}2.7]$$

where k_5' $(= \sqrt{k_5/[O_i^{-2}]}\ )$ is a constant. Therefore according to the above model the p-type conductivity is proportional to $P_{O_2}^{1/4}$.

The excess electrons are expected to be produced at low P_{O_2} according

to the following reaction

$$O_O = 1/2\ O_2\ (gas) + V_O^2 + 2\ e^{-1} \qquad [A\text{-}2.8]$$

where e^{-1} is an excess electron with a valence of -1.

The equilibrium constant for the reaction [A-2.8] is given by

$$k_8 = P_{O_2}^{1/2}\ [V_O^2]\ [e^{-1}]^2 \qquad [A\text{-}2.9]$$

Because $[V_O^2]$ is effectively constant over the P_{O_2} range under consideration

$$[e^{-1}] \propto P_{O_2}^{-1/4} \qquad [A\text{-}2.10]$$

Therefore the n-type conductivity should be proportional to -1/4 as postulated by Lasker and Rapp (43).

APPENDIX B-1. ELECTRICAL CONDUCTIVITY DATA

Run 1. Thoria (Batch 1) in oxygen at 1 atm.

Temperature °C	Log σ (mho/cm)
806	- 5.13
898	- 4.54
947	- 4.27
711	- 5.81
850	- 4.81
992	- 4.02
1064	- 3.68

Run 2. Thoria (Batch 1) in oxygen at 1 atm.

993	- 3.97
892	- 4.48
798	- 5.04
697	- 5.79

Run 3. Thoria (Batch 1) in He/O_2 ratio = 1/100

1066	- 4.18
990	- 4.52
891	- 5.09
753	- 6.16

Run 4. Thoria (Batch 1) in He/O_2 ratio = 1/100

999	- 4.50
897	- 5.02
800	- 5.67
699	- 6.58

Temperature °C	Log σ (mho/cm)
Run 5. Thoria (Batch 1) in CO_2/CO ratio = 1	
1000	- 5.67
897	- 6.36
800	- 7.10
712	- 7.74
Run 6. Thoria (Batch 1) in CO_2/CO ratio = 0.01	
996	- 5.70
897	- 6.37
800	- 7.11
997	- 5.70
Run 7. Cu, Cu_2O/Thoria (Batch 1)/Cu, Cu_2O	
920	- 5.82
963	- 5.55
790	- 7.08
970	- 5.55
1003	- 5.31
967	- 5.57
918	- 5.96
869	- 6.36
Run 8. Co, CoO/Thoria (Batch 1)/Co, CoO	
961	- 5.99
998	- 5.75
1056	- 5.40
1099	- 5.13
903	- 6.44
953	- 6.06
1002	- 5.73

Run 8. (Continued)

Temperature °C	Log σ (mho/cm)
1050	- 5.41
1076	- 5.26
869	- 6.71

Run 9A. Mn, MnO/Thoria (Batch 1)/Mn, MnO

1071	- 5.05
999	- 5.49
941	- 5.92
904	- 6.22
809	- 7.07

Run 9B. Mn, MnO/Thoria (Batch 1)/Mn, MnO

1071	- 4.98
999	- 5.40
941	- 5.85
904	- 6.15
809	- 7.00

Run 10. Ti, TiO/Thoria (Batch 1)/Ti, TiO

1076	- 2.85
982	- 3.35
1073	- 2.90
840	- 4.27
695	- 5.48
998	- 3.28
947	- 3.56
899	- 3.88
800	- 4.58

Temperature °C	Log σ (mho/cm)
Run 11A. Thoria (Batch 2) in oxygen at 1 atm.	
995	- 3.85
898	- 4.32
798	- 4.90
702	- 5.61
606	- 6.45
753	- 5.20
851	- 4.57
950	- 4.04
1043	- 3.64
Run 11B. Thoria (Batch 2) in oxygen at 1 atm.	
995	- 3.86
898	- 4.34
798	- 4.92
702	- 5.62
606	- 6.45
753	- 5.21
851	- 4.58
950	- 4.05
1043	- 3.66
Run 12A. Thoria (Batch 2) in oxygen at 1 atm.	
992	- 3.98
897	- 4.41
794	- 5.01
702	- 5.69

Temperature °C	Log σ (mho/cm)
Run 12B. Thoria (Batch 2) in oxygen at 1 atm.	
992	- 3.99
897	- 4.41
794	- 5.01
702	- 5.68
Run 13A. Thoria (Batch 2) in He/O_2 ratio = 1/100	
1042	- 4.19
993	- 4.40
947	- 4.62
898	- 4.87
847	- 5.13
751	- 5.80
655	- 6.62
Run 13B. Thoria (Batch 2) in He/O_2 ratio = 1/100	
1042	- 4.22
993	- 4.42
947	- 4.64
898	- 4.89
847	- 5.15
751	- 5.81
655	- 6.62
Run 14A. Thoria (Batch 2) in CO_2/CO ratio = 1	
995	- 5.49
795	- 6.82
704	- 7.48
899	- 6.09

Temperature °C	Log σ (mho/cm)
Run 14B. Thoria (Batch 2) in CO_2/CO ratio = 1	
995	- 5.42
795	- 6.78
704	- 7.42
899	- 6.07
Run 15A. Thoria (Batch 2) in CO_2/CO ratio = 0.01	
989	- 5.50
898	- 6.10
796	- 6.84
704	- 7.52
Run 15B. Thoria (Batch 2) in CO_2/CO ratio = 0.01	
989	- 5.52
898	- 6.09
796	- 6.80
704	- 7.46
Run 16A. Cu, Cu_2O/Thoria (Batch 2)/Cu, Cu_2O	
998	- 5.11
949	- 5.43
903	- 5.76
850	- 6.17
803	- 6.56
749	- 7.04
703	- 7.44
Run 16B. Cu, Cu_2O/Thoria (Batch 2)/Cu, Cu_2O	
998	- 5.09
949	- 5.41

Temperature °C	Log σ (mho/cm)
Run 16B. (Continued)	
903	- 5.74
850	- 6.15
803	- 6.54
749	- 7.04
703	- 7.46
Run 17A. Cu, Cu_2O/Thoria (Batch 2)/Cu, Cu_2O	
790	- 6.74
880	- 5.98
975	- 5.27
1006	- 5.06
880	- 5.94
790	- 6.68
701	- 7.46
789	- 6.70
1007	- 5.05
836	- 6.29
Run 17B. Cu, Cu_2O/Thoria (Batch 2)/Cu, Cu_2O	
790	- 6.73
880	- 5.96
975	- 5.27
1006	- 5.07
880	- 5.93
790	- 6.68
701	- 7.48
789	- 6.70
1007	- 5.05
836	- 6.29

Temperature °C	Log σ (mho/cm)
Run 18A. Ni, NiO/Thoria (Batch 2)/Ni, NiO	
999	- 5.50
1090	- 5.06
895	- 6.22
797	- 6.99
696	- 7.77
845	- 6.57
945	- 5.89
1041	- 5.32
745	- 7.41
Run 18B. Ni, NiO/Thoria (Batch 2)/Ni, NiO	
999	- 5.59
1090	- 5.11
895	- 6.22
797	- 7.06
696	- 7.90
845	- 6.59
945	- 5.90
1041	- 5.37
745	- 7.58
Run 19A. Ni, NiO/Thoria (Batch 2)/Ni, NiO	
992	- 5.45
1092	- 4.88
986	- 5.48
894	- 6.08
795	- 6.81
995	- 5.43
791	- 6.82

Temperature °C	Log σ (mho/cm)
Run 19B. Ni, NiO/Thoria (Batch 2)/Ni, NiO	
992	- 5.42
1042	- 4.85
986	- 5.45
894	- 6.05
795	- 6.77
995	- 5.40
791	- 5.79
Run 20. Nb, NbO/Thoria (Batch 2)/Nb, NbO	
858	- 6.35
811	- 6.72
906	- 6.04
954	- 5.72
1002	- 5.41
905	- 6.06
1002	- 5.42
858	- 6.42
Run 21. Nb, NbO/Thoria (Batch 2)/Nb, NbO	
980	- 5.50
935	- 5.76
886	- 6.08
840	- 6.42
790	- 6.78
746	- 7.18
981	- 5.51
1029	- 5.29
884	- 6.12
780	- 6.87
699	- 7.57

Temperature °C	Log σ (mho/cm)
Run 22. Ti, TiO/Thoria (Batch 2)/Ti, TiO	
1050	- 3.84
954	- 4.43
858	- 5.14
905	- 4.77
954	- 4.43
1000	- 4.04

APPENDIX B-2. OPEN CIRCUIT EMF DATA

Cell: Ti, TiO/Thoria/Nb, NbO

Temperature °C	Emf, Volts	Temperature °C	Emf, Volts
(Batch 1)			
753	0.089	937	0.076
763	0.083	942	0.054
782	0.079	947	0.068
807	0.070	952	0.074
817	0.088	982	0.058
817	0.086	982	0.061
842	0.077	985	0.065
897	0.080	986	0.066
900	0.066	987	0.070
901	0.064	987	0.074
910	0.065	1042	0.064
912	0.072	1048	0.054
920	0.068	1092	0.064
935	0.071		
(Batch 2)			
755	0.145	900	0.112
775	0.134	907	0.118
800	0.138	907	0.108
842	0.118	907	0.106
850	0.137	932	0.122
860	0.107	942	0.105
860	0.102	950	0.117
860	0.101	950	0.115
895	0.123	957	0.111
897	0.119	962	0.120

Temperature °C	Emf, Volts	Temperature °C	Emf, Volts
Batch 2 (continued)			
962	0.107	1002	0.107
987	0.125	1017	0.112
987	0.106	1032	0.109
990	0.111	1055	0.107

APPENDIX B-3. THERMOGRAVIMETRIC MEASUREMENTS OF THORIUM IN OXYGEN AT 1 ATM.

Run 1. Temperature = 800°C

Surface area of specimen = 1.1936 sq. cm.

Time (t), min	$\sqrt{t}$, min$^{1/2}$	Weight gain, mgms
0	0	0
1	1	0.2
4	2	0.5
9	3	0.8
16	4	1.15
25	5	1.55
36	6	1.95
49	7	2.20
64	8	2.62
81	9	3.00
100	10	3.40

Run 2. Temperature = 900°C

Surface area of specimen = 1.2555 sq. cm.

Time (t), min	$\sqrt{t}$, min$^{1/2}$	Weight gain, mgms
0	0	0
1	1	0.37
4	2	1.0
9	3	1.6
16	4	2.2
25	5	2.9
36	6	3.6
49	7	4.36
64	8	5.0

Run 2. (Continued)

Time (t), min	$\sqrt{t}$, $min^{1/2}$	Weight gain, mgms
81	9	5.7
100	10	6.4

Run 3. Temperature = 1000°C

Surface area of specimen = 1.2945 sq. cm.

Time (t), min	$\sqrt{t}$, $min^{1/2}$	Weight gain, mgms
0	0	0
1	1	1.0
4	2	2.2
9	3	3.6
16	4	4.9
25	5	6.2
36	6	7.6
49	7	8.8
64	8	10.2
81	9	11.4
100	10	12.6

Run 4. Temperature = 1100°C

Surface area of specimen = 1.3911 sq. cm.

Time (t), min.	$\sqrt{t}$, $min^{1/2}$	Weight gain, mgms
0	0	0
1	1	1.8
4	2	4.0
9	3	5.8
16	4	7.2

Run 4. (Continued)

Time (t), min	$\sqrt{t}$, $min^{1/2}$	Weight gain, mgms
25	5	9.0
36	6	10.8
49	7	12.0
64	8	13.6

APPENDIX C-1.

FORTRAN COMPUTER PROGRAM

FOR THE DETERMINATION OF LOG P_{θ}

FROM EMF DATA

```
C      THIS PROGRAM CALCULATES THE LEAST-SQUARE BEST FIT FOR THE LOGP-
C      NEGATIVE OF THORIA FROM OBSERVED EMFS BETWEEN NB,NBO AND TI,TIO
C      ELECTRODES.
       DIMENSION X(100),Y(100)
       READ(1,100)ZPOS,QPOS,PL,QPL,PR,QPR
C      ZPOS=COMMON LOGARITHM OF THE PRE-EXPONENTIAL OF P-POSITIVE.
C      QPOS=ACTIVATION ENERGY OF P-POSITIVE.
C      PL=COMMON LOGARITHM OF THE PRE-EXPONENTIAL OF THE OXYGEN PARTIAL
C      PRESSURE FIXED BY NB,NBO ELECTRODE=7.29.
C      QPL=ACTIVATION ENERGY OF THE OXYGEN PARTIAL PRESSURE FIXED BY
C      NB,NBO ELECTRODE=190905.74.
C      PR=COMMON LOGARITHM OF THE PRE-EXPONENTIAL OF THE OXYGEN PARTIAL
C      PRESSURE FIXED BY TI,TIO ELECTRODE=9.46.
C      QPR=ACTIVATION ENERGY OF THE OXYGEN PARTIAL PRESSURE FIXED BY
C      TI,TIO ELECTRODE=245257.73.
C      ALL PRESSURES IN ATMOSPHERES. ALL ACTIVATION ENERGIES IN CALS/MOLE
       READ(1,200)N,W
C      W=0.25 CHARACTERIZING THE OXYGEN PARTIAL PRESSURE DEPENDENCE OF
C      ELECTRONIC CONDUCTIVITY.
       WRITE(3,300)
       DO 500 I=1,N
       READ(1,400)EMF,TEMP
C      EMF=OBSERVED EMF IN VOLTS, TEMP= TEMPERATURE IN DEGREE C.
       ATEMP=TEMP+273.
       BPOS=ZPOS-QPOS/(4.575*ATEMP)
       BPL=PL-QPL/(4.575*ATEMP)
       BPR=PR-QPR/(4.575*ATEMP)
       APOS=10.**(BPOS*W)
       APL=10.**(BPL*W)
       APR=10.**(BPR*W)
       A=10.**((EMF*23062.)/(4.575*ATEMP)-ALOG10((APOS+APR)/(APOS+APL)))
       Y(I)=ALOG10((A*APR-APL)/(1.-A))/W
       X(I)=10000./ATEMP
  500  WRITE(3,600)EMF,TEMP,Y(I),X(I)
       B=0.
       C=0.
       D=0.
```

```
      E=0.
      DO 700 I=1,N
      B=B+(X(I)*Y(I))
      C=C+X(I)
      D=D+Y(I)
      E=E+(X(I)**2.)
  700 CONTINUE
      F=N
      QA=((F*B)-(C*D))/((F*E)-(C**2.))
      PZERO=(D-(QA*C))/F
      Q=QA*45750.
C     Q=ACTIVATION ENERGY OF P-NEGATIVE, PZERO= COMMON LOGARITHM OF THE
C     PRE-EXPONENTIAL OF P-NEGATIVE.
      WRITE(3,800)QA,PZERO,Q
  100 FORMAT(6(2X,F10.2))
  200 FORMAT(I3,10X,F4.2)
  300 FORMAT(3X,'EMF',12X,'TEMPERATURE',12X,'P-NEGATIVE',15X,'10000/T')
  400 FORMAT(5X,F7.4,5X,F7.2)
  600 FORMAT(1X,F7.4,12X,F7.2,16X,F7.2,16X,F7.2)
  800 FORMAT(1X,'SLOPE=',F12.2,5X,'P-NEGATIVE-ZERO=',F7.2,5X,'ACTIVATION
     1ENERGY=',F12.2)
      STOP
      END
```

APPENDIX C-2.

FORTRAN COMPUTER PROGRAM FOR CALCULATING OXYGEN PERMEABILITY OF THORIA AND RATIONAL OXIDATION (SCALING RATE) CONSTANT OF THORIUM

```
C       THIS PROGRAM CALCULATES THE SCALING RATE CONSTANT OF THORIUM OR
C       THE OXYGEN PERMEABILITY OF THORIA IN MOLES/CM-SEC FROM THE
C       CONDUCTIVITY PARAMETERS OF THORIA.
        DIMENSION X(20),Y(20)
        READ(1,100)SIGZ,QION,ZPOS,QPOS,ZNEG,QNEG
C       SIGZ=COMMON LOGARITHM OF THE PRE-EXPONENTIAL OF THE IONIC
C       CONDUCTIVITY.
C       QION=ACTIVATION ENERGY OF THE IONIC CONDUCTIVITY.
C       ZPOS=COMMON LOGARITHM OF THE PRE-EXPONENTIAL OF P-POSITIVE.
C       QPOS=ACTIVATION ENERGY OF P-POSITIVE.
C       ZNEG=COMMON LOGARITHM OF THE PRE-EXPONENTIAL OF P-NEGATIVE.
C       QNEG=ACTIVATION ENERGY OF P-NEGATIVE.
        READ(1,200)PL,QPL,PR,QPR
C       PL=COMMON LOGARITHM OF THE PRE-EXPONENTIAL OF THE OXYGEN PARTIAL
C       PRESSURE AT THE HIGH SIDE.
C       QPL=ACTIVATION ENERGY OF THE OXYGEN PARTIAL PRESSURE AT THE HIGH
C       SIDE.
C       PR=COMMON LOGARITHM OF THE PRE-EXPONENTIAL OF THE OXYGEN PARTIAL
C       PRESSURE AT THE LOW SIDE.
C       QPR=ACTIVATION ENERGY OF THE OXYGEN PARTIAL PRESSURE AT THE LOW
C       SIDE.
C       ALL PRESSURES IN ATMOSPHERES. ALL ACTIVATION ENERGIES IN CALS/MOLE
        WRITE(3,300)
        WRITE(3,100)SIGZ,QION,ZPOS,QPOS,ZNEG,QNEG
        WRITE(3,301)
        WRITE(3,200)PL,QPL,PR,QPR
        WRITE(3,302)
        READ(1,400)N,W,Z,D
C       W=0.25 CHARACTERIZING THE OXYGEN PARTIAL PRESSURE DEPENDENCE OF
C       ELECTRONIC CONDUCTIVITY.
C       Z=2 THE VALENCE OF OXYGEN ION.
C       D=2 THE NUMBER OF OXYGEN ATOMS PER MOLECULE OF THORIA IN CASE OF
C       SCALING.  THE VALUE OF D IS ALSO 2 THE NUMBER ATOMS/MOLECULE OF
C       GASEOUS OXYGEN IN CASE OF PERMEABILITY.
        DO 500 I=1,N
        READ(1,600)TEMP
C       TEMP=TEMPERATURE IN DEGREE C.
```

```
      TEMP=TEMP+273.
      SIGMA=10.**(SIGZ-QION/(4.575*TEMP))
      BPOS=ZPOS-QPOS/(4.575*TEMP)
      BNEG=ZNEG-QNEG/(4.575*TEMP)
      PK=(BPOS+BNEG)/2.
      BPL=PL-QPL/(4.575*TEMP)
      BPR=PR-QPR/(4.575*TEMP)
      APOS=10.**BPOS
      ANEG=10.**BNEG
      APL=10.**BPL
      APR=10.**BPR
      APK=10.**PK
      A=2.*(APOS**(-W))*(APL**W)
      CA=2.*(APOS**(-W))*(APK**W)
      B=2.*(ANEG**W)*(APR**(-W))
      CB=2.*(ANEG**W)*(APK**(-W))
      H=SQRT(1.-4.*((ANEG/APOS)**W))
      AA=ALOG10((A+1.-H)/(A+1.+H))
      CCA=ALOG10((CA+1.-H)/(CA+1.+H))
      BB=ALOG10((B+1.-H)/(B+1.+H))
      CCB=ALOG10((CB+1.-H)/(CB+1.+H))
      C=4.186*4.575/(2.*D*Z*Z*96500.*96500.)
      F=1./(W*H)
      FUNC=C*TEMP*SIGMA*(BPL-BPR-F*(AA-CCA-CCB+BB))
C     FUNC=(FUNCTION) THE SCALING RATE CONSTANT OR THE PERMEABILITY IN
C     MOLES/CM-SEC.
      X(I)=10000./TEMP
      Y(I)=ALOG10(FUNC)
  500 WRITE(3,700)TEMP,SIGMA,BPOS,BNEG,BPL,BPR,FUNC
      WRITE(3,800)
      S=0.
      T=0.
      U=0.
      V=0.
      DO 750 I=1,N
      S=S+(X(I)*Y(I))
      T=T+X(I)
```

```
      U=U+Y(I)
      V=V+(X(I)**2.)
  750 WRITE(3,900)X(I),Y(I)
      G=N
      QA=((G*S)-(T*U))/((G*V)-(T**2.))
      PZERO=(U-(QA*T))/G
      Q=QA*45750.
      WRITE(3,950)QA,PZERO,Q
  100 FORMAT(6(3X,F10.2))
  200 FORMAT(4(3X,F10.2))
  400 FORMAT(I3,2X,3(5X,F5.2))
  600 FORMAT(F7.2)
  300 FORMAT(3X,'SIGMA-ZERO',5X,'QION',7X,'P-POS-ZERO',3X,'Q-POSITIVE',3
     1X,'P-NEG-ZERO',3X,'Q-NEGATIVE')
  301 FORMAT(3X,'PX2-LEFT',5X,'Q-PX2-LEFT',3X,'PX2-RIGHT',4X,'Q-PX2-RIGH
     2T')
  302 FORMAT(1X,'TEMP-DEGREE-K',4X,'CONDUCTIVITY',6X,'LOG-P-POSITIVE',4X
     3,'LOG-P-NEGATIVE',4X,'LOG-PX2-LEFT',6X,'LOG-PX2-RIGHT',7X,'FUNC')
  700 FORMAT(7(E13.6,5X))
  800 FORMAT(1X,'10000/T',14X,'LOG-FUNCTION')
  900 FORMAT(1X,F7.2,12X,F13.6)
  950 FORMAT(1X,'SLOPE=',F6.2,5X,'INTERCEPT=',F7.2,5X,'ACTIVATION ENERGY
     5=',F12.2)
      STOP
      END
```

ACKNOWLEDGMENT

The author wishes to record his deepest appreciation to Dr. John W. Patterson for his encouragement, guidance and valuable suggestions throughout the course of the present investigation. Thanks are due to Dr. D. T. Peterson for making available the thorium specimens used in the oxidation study. The author is indebted to Mr. C. D. Wirkus for his help and permission to use the apparatus for the thermogravimetric measurements and for the electron probe analyses. Last but not the least, the author is grateful to his wife, Leela, for her patience and support during the investigation.